Geophysica (2016), 51(1), 17–50

Climate Projections for Finland Under the RCP Forcing Scenarios

Kimmo Ruosteenoja[*]*, Kirsti Jylhä and Matti Kämäräinen*

Finnish Meteorological Institute, P.O.Box 503, FI-00101 Helsinki, Finland

* Corresponding author: kimmo.ruosteenoja@fmi.fi

(Received: February 2016; Accepted: April 2016)

Abstract

Climate change projections for Finland have been calculated from simulations performed with 28 recent-generation (CMIP5) global climate models. During the next few decades, projected changes are fairly similar under all four RCP forcing scenarios examined. Conversely, in the second half of this century, the evolution of climate is highly dependent on greenhouse gas emissions. Under the high-emission RCP8.5 forcing scenario for the period 2040–2069, surface air temperatures in winter are projected to increase by 2–7°C relative to 1981–2010, while precipitation would increase by 4–30 % and diurnal temperature range diminish by 5–34 %. For incident solar radiation, the projected change falls between –17 and +2 %. In summer warming is more modest, 1–4°C; for the other quantities, the sign of changes remains uncertain, even though minor increases are likely for both precipitation and solar radiation. For mean temperature and solar radiation, uncertainty in projected changes mainly stems from modelling differences, while for precipitation, the contribution of internal variability is prominent.

Compared to the previous model generation, the new CMIP5 models simulate somewhat larger warming for summer, while the precipitation projections are nearly equal throughout the year. For surface wind speed, the multimodel-mean change is close to zero, in contrast to a slight increase inferred from the previous model generation. However, inter-model differences in the wind speed projections are large, up to ±15%.

The geographical pattern of the modelled change can be downscaled spatially by using regional climate models. However, in the simulations based on a single regional model that were examined here, dynamical downscaling proved to lead to a substantial underestimation of the projection uncertainty for solar radiation and warm-season temperature.

Keywords: CMIP5 models, multimodel climate projections, climate change, surface air temperature, precipitation, solar radiation, diurnal temperature range

1 Introduction

During the coming decades and centuries, global mean temperature is anticipated to rise as a response to the increasing abundances of greenhouse gases in the atmosphere. Global-scale warming will be reflected in the Finnish climate as well.

Indications of the ongoing warming are already apparent in the observations. By fitting a dynamic regression model to the monthly mean temperatures in Finland, *Mikkonen et al.* (2015) found that the country-wide spatially-averaged annual mean temperature in Finland has risen by a total of 2.3 ± 0.4 °C (with 95 % probability limits) during the years 1847–2013. The resulting long-term mean trend of 0.14 °C per decade is near-

ly twice as large as the corresponding increase in global mean temperature. In Finland, warming has occurred in two periods, from the 1850s to the late 1930s and from the end of the 1960s to the present. The change has been largest in November, December and January. Also, the spring months from March to May have warmed more rapidly than the annual average.

Temperature trends in Finland since 1961 have been studied in more detail by *Irannezhad et al.* (2015) and *Aalto et al.* (2016). Owing to some differences in the data and analysis methods, the former paper reported an annual-mean warming trend of 0.4 ± 0.2 and the latter 0.3 ± 0.2 °C per decade. According to *Aalto et al.* (2016), the mean daily maximum and minimum temperatures have increased by 0.3 ± 0.2 °C and 0.4 ± 0.2 °C per decade, respectively. Snow depth was reported to have decreased, on average, by 1.2 ± 0.5 cm per decade, whereas no statistically significant trends were detected in the country-wide spatial averages of precipitation and surface air pressure. In autumn in southern Finland, the total solar radiation had increased by 5 % per decade during 1980–2009 (*Jylhä et al.*, 2014).

Estimates for future climatic changes can be inferred from simulations performed with global climate models (GCMs). To enhance the robustness of the projections and permit credible uncertainty analyses, it is necessary to examine a sufficiently wide set of models. For that purpose, international data archives have been constructed from which climate scientists can download output data from state-of-the-art models. Among these archives, the data banks of the Coupled Model Intercomparison Project (CMIP) play a key role. In order to ensure that data from the most recent model generation is always provided, the CMIP archives are updated approximately at six-year intervals, in phase with the publication of the assessment reports of the Intergovernmental Panel on Climate Change (IPCC).

The sustained evolution of climate models affects their ability to simulate both the recent past climate and forthcoming changes arising as a response to the increasing greenhouse gas forcing. Accordingly, as a new model generation becomes available, climate change projections need to be revised, both on global and regional scales. The main purpose of the present work is to provide updated climate projections for Finland that are based on the most recent CMIP5 climate model ensemble (*Taylor et al.*, 2012), i.e., the manifold of GCMs that was utilized in the preparation of the Fifth Assessment Report of *IPCC* (2013). In tandem with introducing this new model generation, reformed greenhouse gas scenarios, Representative Concentration Pathways (RCPs), have been adopted. The philosophy behind the RCP forcing scenarios is discussed in detail in *van Vuuren et al.* (2011).

Previously, scenarios for future climatic conditions in Finland have been developed within the framework of the Finnish Research Programme on Climate Change SILMU (*Carter et al.*, 1996; *Fortelius et al.*, 1996); in the FINSKEN project (*Jylhä et al.*, 2004) as a part of the Finnish Global Change Research Programme FIGARE; in the FINADAPT project (*Carter et al.*, 2005; *Ruosteenoja et al.*, 2005); and in the two phases of the ACCLIM project (*Jylhä et al.*, 2009; *Ruosteenoja et al.*, 2013) of the National Climate Change Adaptation Research Programme ISTO. In the ACCLIM project, the

climate projections were calculated from the previous-generation CMIP3 climate model simulations[1]. Climate change scenarios derived from the CMIP3 GCMs are also available for countries adjacent to Finland, e.g., for Russia (*Meleshko et al.*, 2008), Sweden (*Lind and Kjellström*, 2008) and Estonia (*Jaagus and Mändla*, 2014).

Climate change scenarios framed in the ACCLIM project have been utilized widely in climate change impact, adaptation and vulnerability research in Finland. Recent examples of those studies include, among others, assessing future changes in forest growth (*Mäkipää et al.*, 2015; *Torssonen et al.*, 2015), forest fire risks (*Lehtonen et al.*, 2014), forest carbon stock (*Sievänen et al.*, 2014), crop yield potentials (*Peltonen-Sainio et al.*, 2015), reindeer husbandry (*Turunen et al.*, 2016), nutrient loading to the Baltic Sea (*Huttunen et al.*, 2015), greenhouse gas fluxes in peatlands (*Gong et al.*, 2013), sea level in the Baltic Sea (*Johansson et al.*, 2014), heating and cooling energy demand (*Jylhä et al.*, 2015) and temperature-related mortality and vulnerability of elderly people (*Carter et al.*, 2014). In addition, these scenarios have been utilized for the purpose of raising awareness on the severity of the climate change problem (e.g., via the "climateguide.fi" web portal) and for the development of adaptation strategies and the formulation of climate policy on national, regional and municipal level (*Juhola*, 2010; *Ruuhela*, 2011; *Pilli-Sihvola et al.*, 2014).

Also, projections inferred from the CMIP5 GCMs have already been utilized in a few studies in Finland. For example, using these model simulations, *Luomaranta et al.* (2014) reported a substantial future decline in the wintertime ice extent and thickness in the Baltic Sea. Projections for the length and degree-day sum of the thermal growing season have been calculated by *Ruosteenoja et al.* (2015) who inferred that under unabated greenhouse gas emissions, growing degree-day sum in Finland would approximately double by the end of the 21st century (Fig. S14 in the supplement file of this paper).

One aim of the present work is to facilitate the comparison of previous climate change impact and adaptation studies to those based on the recent CMIP5 model generation. For this purpose, we explored briefly to what extent the present projections deviate from projections calculated from the CMIP3 models.

In the current CMIP5 GCMs, the horizontal grid size typically varies between 100 and 300 km. This resolution is adequate for simulating climate at large scales, but the impact of small-scale geographical details remains unresolved. To resolve such fine-scale features, regional climate models (RCMs) have been developed. In this work, we briefly compared GCM-simulated climate change projections for Finland to those derived from selected RCM simulations participating in the EURO-CORDEX initiative (*Jacob et al.*, 2014). It should be emphasized that a RCM is not an independent agent but the resulting climate simulations are largely determined by the boundary data adopted from a driving GCM. There is only a limited number of GCMs for which regionally-downscaled RCM simulations have been published. Hence, the available RCM simula-

[1] CMIP3 models contributed to the previous (fourth) *IPCC* (2007) report while the CMIP5 model ensemble was used in the recent Fifth Assessment Report (*IPCC*, 2013); in these concepts, CMIP4 has been bypassed in the numbering.

tions cannot provide an adequate picture of the true modelling uncertainties. Therefore, to be able to perform a comprehensive uncertainty analysis, we primarily grounded our climate projections on global models.

In assessing the robustness of the projections, we focused on those two sources of uncertainty that are beyond the power of human decision: unforced internal variability and modelling differences. The third key component of uncertainty is due to the unknown future evolution of the human-induced emissions of greenhouse gases and precursors of aerosol particles. We considered this factor of uncertainty by providing climate change projections separately for four alternative greenhouse gas scenarios.

The focus of this paper is on modelled changes in the monthly, seasonal and annual means of surface air temperature, precipitation and incident solar radiation; these variables have a great practical importance, and simulations for them are available from all the GCMs examined. In addition, less extensive analyses are presented for surface air pressure, scalar wind speed and the diurnal range of temperature. First, we discuss the new greenhouse gas scenarios, introduce the climate models analyzed and describe the methodology that was utilized in creating the climate projections.

Thereafter, we examine the temporal evolution and seasonal cycle of projected changes in the climate quantities under different greenhouse gas forcing scenarios. Moreover, the geographical distribution of the responses and the mutual dependencies among changes projected for the various quantities are studied and the new projections are compared with those inferred from the previous model generation. Finally, the GCM-simulated projections are compared with the corresponding dynamically downscaled products. The paper is intended to serve as a reference for researchers from various disciplines who utilize the present climate change projections in their applications; consequently, the paper should be readable for non-climatologists as well. For this purpose, only fairly standard statistical analyses have been presented and the mathematical details of the methodology have been shifted into the Appendix.

2 Methodology

2.1 Greenhouse gas scenarios

In the model runs examined in the present work, the future evolution of the greenhouse gas (carbon dioxide, methane, etc.) and aerosol particle concentrations was extracted from four alternative forcing scenarios. The time series of the emissions and atmospheric concentrations for the most important anthropogenic greenhouse gas, carbon dioxide, under these RCP scenarios are shown in Fig. 1. Under the RCP8.5 scenario[2], emissions continue to increase throughout the 21st century, ultimately nearly threefolding compared to the level that prevailed in 2000, and the concentration of CO_2 would approach 1000 ppm by 2100. According to the other three scenarios, global emissions start to decline during this century. If the RCP4.5 scenario is realized, the CO_2 concentration stabilizes close to 540 ppm, a level about double that in the prein-

[2] The label after the acronym RCP refers to the total radiative forcing (in Wm^{-2}) near the year 2100.

dustrial era. Under the most gentle RCP2.6 scenario, the concentrations start to diminish after mid-century.

Besides the new RCP scenarios, Fig. 1 shows the global emissions and concentrations of CO_2 for three SRES scenarios. These SRES scenarios, A2, A1B and B1, are those most commonly used in the previous GCM simulations and adaptation studies (*IPCC*, 2007). One can see that in the SRES B1 and RCP4.5 scenarios both the emissions and atmospheric abundances of CO_2 match closely. Conversely, for the other two SRES scenarios no analogy can be found among the RCP scenarios; for A1B and A2, the CO_2 concentrations are distinctly above RCP6.0 but below RCP8.5 for the entire century. The same conclusions can be drawn by comparing the evolution of the total radiative forcing that includes the contributions of all radiatively active constituents, including the diverse greenhouse gas and aerosol particle categories (Fig. 1.15 of *IPCC*, 2013).

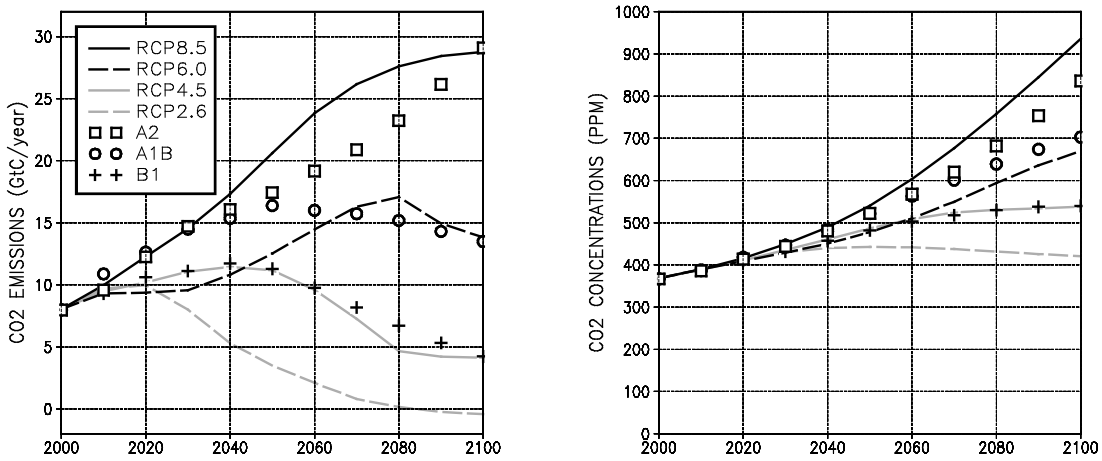

Fig. 1. Temporal evolution of the global emissions (gigatonnes of carbon per year; left panel) and atmospheric abundance (parts per million in volume; right panel) of carbon dioxide in 2000–2100 according to four RCP scenarios (curves) and three SRES scenarios (discrete symbols); see the legend.

2.2 Climate model data

The CMIP5 GCMs analyzed in this study are listed in Table 1. For further information about the individual models and key references, see Table 9.A.1 of *IPCC* (2013).

In the embryo of the present project, we examined 35 GCMs but, following *Luomaranta et al.* (2014), seven of those models were excluded from the present analysis. These rejected models either failed to reproduce the recent past climate in Europe, gave severely-biased simulated temperature trends during the instrumental period or produced future temperature responses to the various RCP scenarios that were mutually inconsistent. Accordingly, 28 models were used in calculating surface air temperature, precipitation, surface air pressure and solar radiation projections under RCP4.5 and RCP8.5 (Table 1). For the other two forcing scenarios, the number of models providing data was smaller: 21 for RCP2.6 and 15 for RCP6.0. For the daily maximum and mini-

mum temperatures and wind speed, data were lacking from a few models. Moreover, in both versions of the IPSL model, diurnal temperature range proved to be unrealistically large, and therefore these models were not considered in studying the daily temperature minima and maxima. Consequently, 25 GCMs were examined for the diurnal temperature cycle and 24 GCMs for wind speed (for RCP4.5 and 8.5).

Changes in daily temperature maxima and minima will not be reported separately. Rather, we analyzed the diurnal temperature range that was obtained as the difference between these two quantities.

Model simulations were forced by the observational "historical" greenhouse-gas concentrations up to the year 2005, after which the concentrations were adopted from a selected RCP scenario. We analyzed model output data until 2099, which constitutes the termination year for some model runs.

Many GCMs provide multiple parallel runs for single RCP scenarios, the maximum count of these being six (Table 1). Parallel runs are forced by identical greenhouse gas and aerosol concentrations, but the initial conditions diverge. As will be demonstrated in the next subsection, differences among the parallel runs can be utilized in assessing the contribution of unforced internal variability to the total uncertainty of future projections.

Dynamically downscaled data were analyzed for those nine GCMs marked in Table 1. The downscaled simulations have been run at a 50 km resolution by the RCA4 RCM, developed at the Rossby Centre of the Swedish Meteorological and Hydrological Institute (*Strandberg et al.*, 2014). The RCP4.5 and RCP8.5 simulations were available, with only a single parallel RCM run for each driving GCM and RCP scenario.

2.3 Processing of the model output

The computational grid varies among the 28 GCMs. Therefore, in calculating the multi-model statistics, all model data were interpolated bi-linearly onto a common 2.5 x 2.5 degree latitude-longitude grid. Thereafter, spatial averages over Finland were calculated as an area-weighted mean of 11 grid boxes covering the country. Henceforth, if not stated otherwise, climate projections for Finland refer to those regional averages. For analyzing the RCM data, we used a finer 0.5 x 0.5 degree grid.

Future changes in the climate variables were calculated relative to the baseline-period 1981–2010 mean. This is the most recent 30-year period for which observational climate statistics have been compiled (*Pirinen et al.*, 2012). This baseline period is also analogous to the 20-year reference period 1986–2005 employed by *IPCC* (2013). As an exception, in comparing the previous CMIP3-inferred climate projections with their present updated counterparts, the baseline period was 1971–2000.

Table 1. Global climate models used in creating climate projections for Finland. The first and second columns state the model acronym and the country of origin; the EC-EARTH model has been developed by a consortium of several European countries. Columns 3–6 give, for each RCP scenario, the number of parallel runs for temperature, precipitation and surface pressure simulations (for the three remaining variables, the number of runs is different for some models). Next, there is a list of variables for which data have been analyzed in the present work for each individual model (T: surface air temperature; PR: precipitation; PSL: sea level pressure; SOL: incident solar radiation at the surface; TXN: difference of the daily maximum and minimum temperatures; W: surface air wind speed). The last column tells the availability of the model output downscaled by the RCA4 model.

Model	Country	$N_{2.6}$	$N_{4.5}$	$N_{6.0}$	$N_{8.5}$	Variables	RCA4
MIROC5	Japan	3	3	1	3	T, PR, PSL, SOL, TXN, W	X
MIROC-ESM	Japan	1	1	1	1	T, PR, PSL, SOL, TXN, W	
MIROC-ESM-CHEM	Japan	1	1	1	1	T, PR, PSL, SOL, TXN, W	
MRI-CGCM3	Japan	1	1	1	1	T, PR, PSL, SOL, TXN, W	
BCC-CSM1-1	China	1	1	1	1	T, PR, PSL, SOL, TXN, W	
INMCM4	Russia	-	1	-	1	T, PR, PSL, SOL, TXN, W	
NorESM1-M	Norway	1	1	1	1	T, PR, PSL, SOL, TXN	X
NorESM1-ME	Norway	1	1	1	1	T, PR, PSL, SOL	
HadGEM2-ES	U.K.	4	4	3	4	T, PR, PSL, SOL, TXN, W	X
HadGEM2-CC	U.K.	-	1	-	3	T, PR, PSL, SOL, TXN, W	
MPI-ESM-LR	Germany	3	3	-	3	T, PR, PSL, SOL, TXN, W	X
MPI-ESM-MR	Germany	1	3	-	1	T, PR, PSL, SOL, TXN, W	
CNRM-CM5	France	1	1	-	5	T, PR, PSL, SOL, TXN, W	X
IPSL-CM5A-LR	France	4	4	1	4	T, PR, PSL, SOL, W	
IPSL-CM5A-MR	France	1	1	-	1	T, PR, PSL, SOL, W	X
CMCC-CM	Italy	-	1	-	1	T, PR, PSL, SOL, TXN, W	
CMCC-CMS	Italy	-	1	-	1	T, PR, PSL, SOL, TXN, W	
GFDL-CM3	U.S.A.	1	1	1	1	T, PR, PSL, SOL, TXN, W	
GFDL-ESM2M	U.S.A.	1	1	1	1	T, PR, PSL, SOL, TXN, W	X
GISS-E2-R	U.S.A.	1	5	1	1	T, PR, PSL, SOL, TXN, W	
GISS-E2-H	U.S.A.	1	5	1	1	T, PR, PSL, SOL, TXN, W	
NCAR-CCSM4	U.S.A.	5	6	6	6	T, PR, PSL, SOL, TXN	
NCAR-CESM1-CAM5	U.S.A.	3	3	3	3	T, PR, PSL, SOL, TXN, W	
NCAR-CESM1-BGC	U.S.A.	-	1	-	1	T, PR, PSL, SOL, TXN	
CanESM2	Canada	5	5	-	5	T, PR, PSL, SOL, TXN, W	X
ACCESS1-0	Australia	-	1	-	1	T, PR, PSL, SOL, TXN, W	
ACCESS1-3	Australia	-	1	-	1	T, PR, PSL, SOL, TXN, W	
EC-EARTH	Europe	2	6	-	6	T, PR, PSL, SOL, TXN, W	X

As can be seen in the matrix of model runs (Table 1), simulations for RCP4.5 and RCP8.5 have been conducted by all GCMs. For the other two scenarios, there are gaps in the matrix, i.e., runs are lacking from a number of models. In order to make the future projections mutually comparable for all the RCP scenarios, these gaps were filled by employing a modification of the pattern-scaling technique developed in *Ruosteenoja et al.* (2007). The details of the procedure are described in section A1 in the Appendix.

In calculating the multi-model means and standard deviations for the simulated changes, all 28 GCMs were weighted equally, with the exception that no individual research centre was given more than two votes. Accordingly, halved weight coefficients were given for MIROC-ESM, MIROC-ESM-CHEM, CESM1-CAM5 and CESM1-BGC, while the remaining GCMs were weighted by unity. As discussed in *Weigel et al.* (2010), non-equal weighting would be justifiable only if we had compelling quantitative

information about the performance of individual models in simulating future climate. Furthermore, *Räisänen and Ylhäisi* (2015) found no statistically significant correlation between biases in the simulated baseline climate and in the modelled future change. Thus, the performance of a model in simulating observed climate yields little information about its ability to forecast future changes.

For any individual RCP scenario, the uncertainty of future changes in a climate variable (e.g., temperature) consists of two components, modelling uncertainty and internal natural variability. *Ruosteenoja et al.* (2015) derived equations that can be used to decompose the total variance of uncertainty into these two components. This can be done by inspecting the parallel run mean changes and deviations thereof. This exercise is outlined in section A2 in the Appendix.

After calculating the standard deviations of the total projection uncertainty, 90 % uncertainty intervals for the change were calculated by using the normality approximation.

3 Climate projections

3.1 Temporal mean changes

The temporal evolution of annual mean temperature and precipitation sum in Finland is depicted in Fig. 2. Annual and seasonal multi-model mean changes are given for all six variables in Tables S1–S6 of the supplement file.

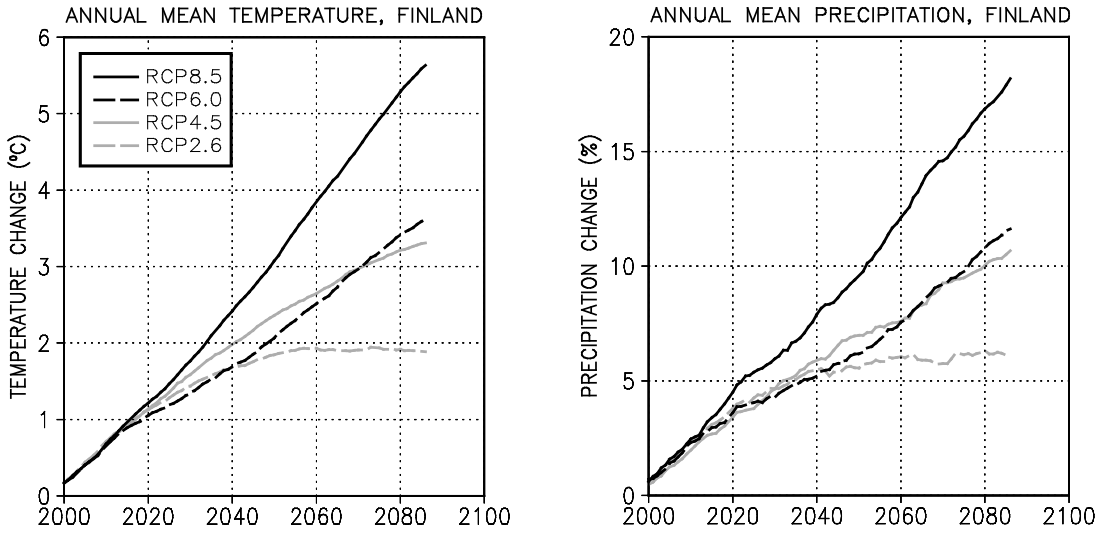

Fig. 2. Projected multi-model mean changes in annual mean surface air temperature (in °C; left panel) and precipitation (in %; right panel) for the years 2000–2085, relative to the mean of the baseline period 1981–2010. All values are 30-year running means averaged spatially over Finland. Projections are depicted separately for four greenhouse gas scenarios: RCP8.5, RCP6.0, RCP4.5 and RCP2.6 (see the legend).

During the next few decades, both the annual mean temperature and precipitation will increase in Finland at a similar rate according to all four RCP scenarios, but later in this century the projections diverge. By mid-century, the temperature responses to the

most gentle and severe RCP scenarios deviate by about 1°C; by the 2080s, nearly 4°C. An analogous behaviour can be seen in the evolution of the annual precipitation total. If the highly ambitious RCP2.6 scenario were realized, increasing trends in temperature and precipitation would cease after mid-century. According to RCP8.5, by contrast, the tendency towards warmer and wetter conditions would continue almost linearly throughout the century.

The ratio of the annual mean temperature increase in Finland to the global mean increase is projected to range from 1.6 to 1.9 (Table 2). The weaker the global warming, the larger the ratio: thereby, the ratio is largest for RCP2.6 and smallest for RCP8.5, and tends to be highest when studying short-term projections. We hypothesize that this might be related to the retreat of sea ice in the Arctic Ocean. In the early stage of global warming, the edge of the ice still resides fairly close to northern Europe, exerting a substantial cooling influence on the regional climate. As the ice cover melts, this effect gradually attenuates. When the edge has shifted far into the central Arctic Ocean, further retreat does not have this marked impact anymore. Hence, in a relative sense, the local warming effect induced by the vanishing sea ice is largest for weak global warming. This idea is supported by the fact that the contrast among the RCP scenarios and time spans in Table 2 is strongest in spring when the Arctic sea ice cover is most widespread.

Table 2. Seasonal and annual ratios of the projected country-mean temperature increase in Finland to globally averaged warming (both multi-model means). The ratios have been calculated separately for two future periods and four RCP scenarios. DJF: December to February; MAM: March to May; JJA: June to August; SON: September to November; ANN: Annual mean.

PERIOD	SCEN	DJF	MAM	JJA	SON	ANN
2040–2069	RCP2.6	2.2	2.0	1.6	1.7	1.9
	RCP4.5	2.2	1.9	1.5	1.5	1.8
	RCP6.0	2.2	1.8	1.5	1.6	1.8
	RCP8.5	2.2	1.7	1.4	1.6	1.7
2070–2099	RCP2.6	2.1	1.8	1.5	1.6	1.8
	RCP4.5	2.2	1.9	1.4	1.6	1.8
	RCP6.0	2.0	1.7	1.4	1.5	1.7
	RCP8.5	2.0	1.6	1.4	1.5	1.6

The seasonal cycle of projected changes in the six climate variables in Finland is examined in Figs. 3–4 for two future time spans. The earlier period, 2040–2069, is relevant for many climate change adaptation studies, and at that time differences amongst the four RCP scenarios are still rather modest; the other three RCP scenarios project 1.0–1.6°C smaller annual mean warming than RCP8.5 (Fig. 2). Moreover, the mid-century responses to RCP8.5 are close to those projected under RCP4.5 by the late century. The response to RCP8.5 for the late century is intended to act as an alarm signal, demonstrating the furious climatic changes that would be expected if the mitigation of greenhouse gas emissions were totally neglected.

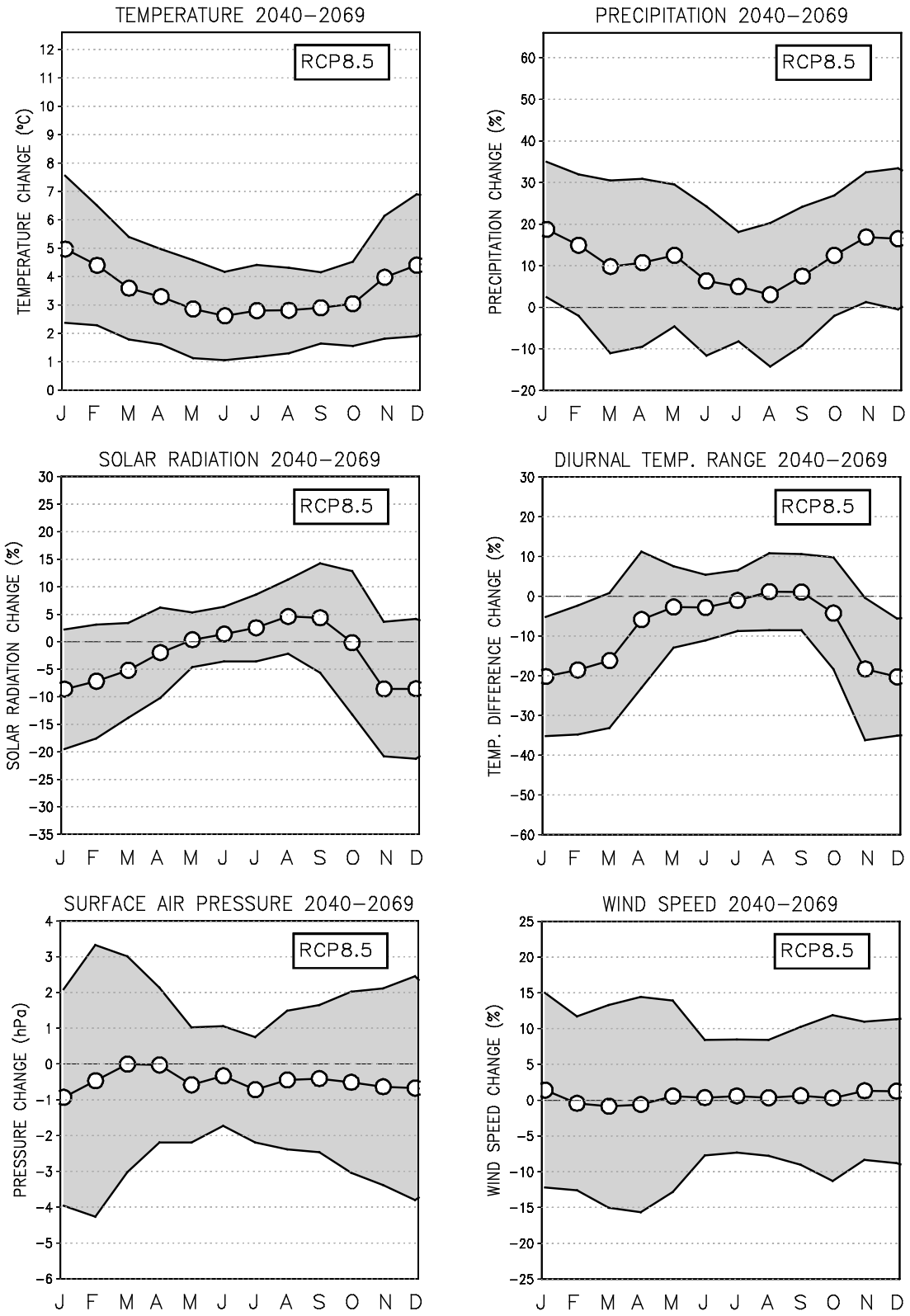

Fig. 3. Projected changes in mean surface air temperature (in °C, top left), precipitation (in %, top right) incident solar radiation (in %, middle left), diurnal temperature range (in %, middle right), surface air pressure (in hectopascals, bottom left) and wind speed (in %, bottom right) in Finland under the RCP8.5 scenario for the period 2040–2069, relative to 1981–2010. The multi-model mean projections for every calendar month (J = January, F = February, ...), based on simulations performed with 24–28 GCMs (see Table 1), are denoted by open circles. Grey shading shows the 90 % uncertainty intervals for the change.

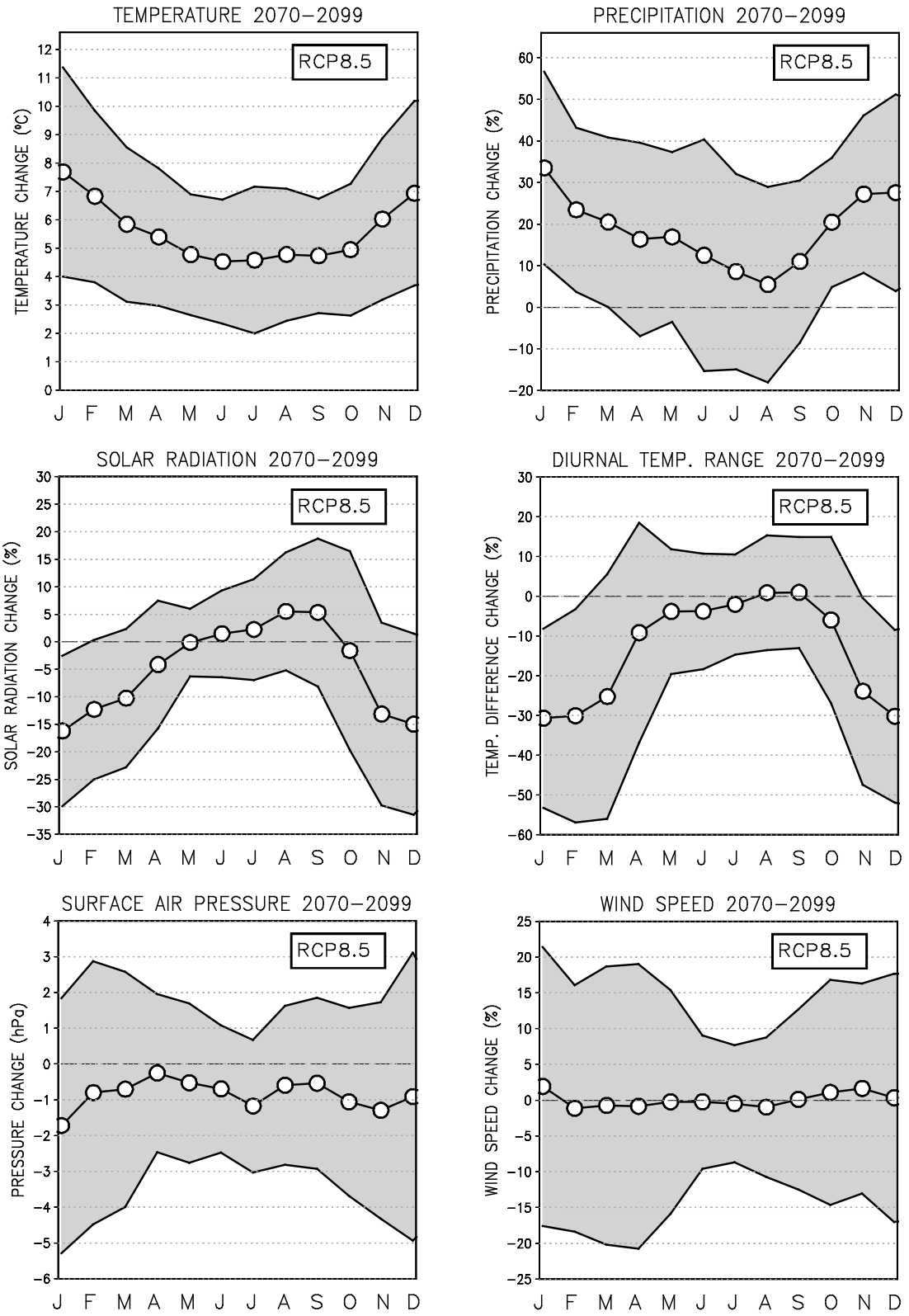

Fig. 4. As in Fig. 3, but for the period 2070–2099 (note the same scale on the vertical axes in Figs. 3 and 4).

Regarding first the multi-model mean (best-estimate) change, warming projected for summer is about 40 % weaker than that simulated for winter: according to RCP8.5, 3°C vs. 5°C for mid- and 5°C vs. 7°C for the late-century period (Figs. 3–4; Table S1). Another key finding is that in winter weather conditions are becoming wetter and darker: by the late 21st century, precipitation is estimated to increase by nearly 30 %, incident solar radiation to decrease by more than 10 % and diurnal temperature range to reduce by 30 % (Tables S2–S4). In summer, projected changes in these three variables are far weaker, and in late summer solar radiation may even increase slightly. A qualitatively similar seasonal dependence is evident also in mid-century.

Besides the best estimates, Figs. 3–4 show the 90 % uncertainty intervals for the change. These uncertainty estimates include both the contribution of inter-model differences and internal variability; see Eq. (7) in the Appendix. Uncertainty intervals were also calculated for the seasonally and annually averaged changes; see Tables S1–S6 in the supplement file.

Models agree on the temperature increase for every season, although the uncertainty intervals appear quite wide; for instance, for the late-century January, warming may attain 11°C, while the best and lower estimates are 8 and 4°C, respectively. In winter, the projected increases in precipitation and decreases in solar radiation and in diurnal variations of temperature are quite robust as well. Conversely, in summer, changes in these three variables may be of either sign; however, both precipitation and insolation are more likely to increase than to decrease.

For surface air pressure and wind speed, model projections for Finland are contradictory, and no robust signal can be detected (Figs. 3–4, lower panels). In particular, for wind speed the best-estimate response is very close to zero throughout the year, but the inter-model scatter is considerable, especially in winter and spring. Accordingly, the CMIP5 model ensemble provides rather little information about future wind conditions, both quite a large weakening and strengthening being possible alternatives.

Geographical distributions of the projections for those four variables that exhibited robust signals in Figs. 3–4 are shown in Figs. 5–8, separately for winter and summer. The whole European continent, rather than merely Finland, is covered. In Figs. 5–8, multi-model means under RCP8.5 are presented for the period 2040–2069, while maps for the periods 2020–2049 and 2070–2099 are given in the supplementary Figs. S4–S11. For all these variables, the geographical distribution of the response appears to be qualitatively similar regardless of the time span explored, with the magnitude of the change being smaller for the earlier periods. This kind of scalability property is very generally valid for climate projections and constitutes the theoretical basis for pattern scaling, a theme discussed in section A1 in the Appendix.

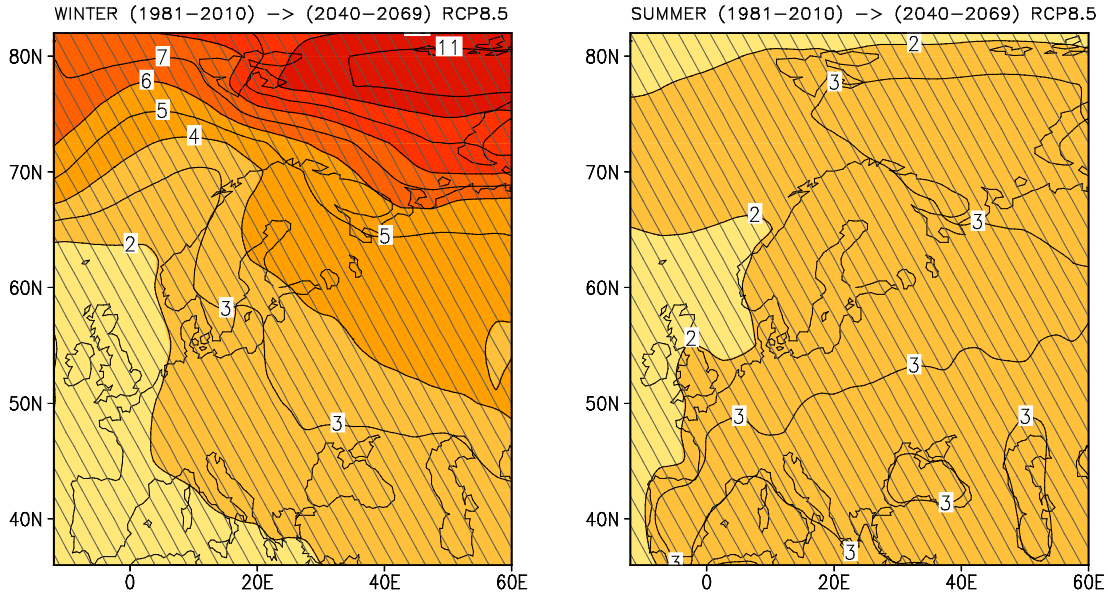

Fig. 5. Projected changes in mean surface air temperature (in °C) in Europe in December-February (left) and June-August (right) under the RCP8.5 scenario for the period 2040–2069, relative to 1981–2010; an average of the simulations performed with the 28 GCMs listed in Table 1. Areas where more than 75 % of the models agree on the sign of change are hatched (for temperature, this condition is fulfilled over the entire domain).

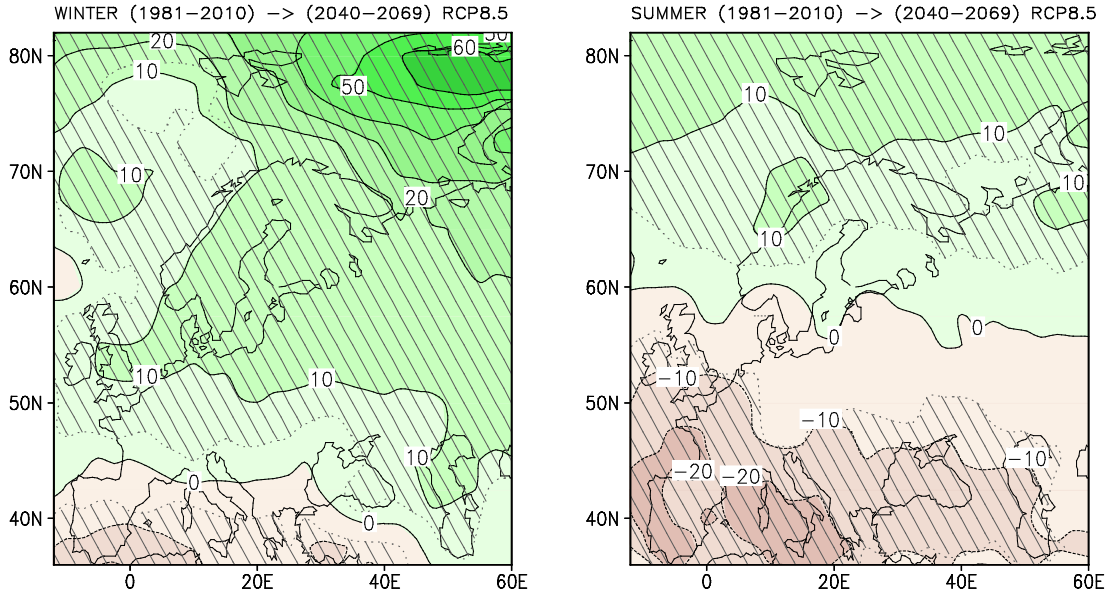

Fig. 6. Projected changes in precipitation totals (in %) in December-February (left) and June-August (right) under the RCP8.5 scenario; for further information, see the caption of Fig. 5.

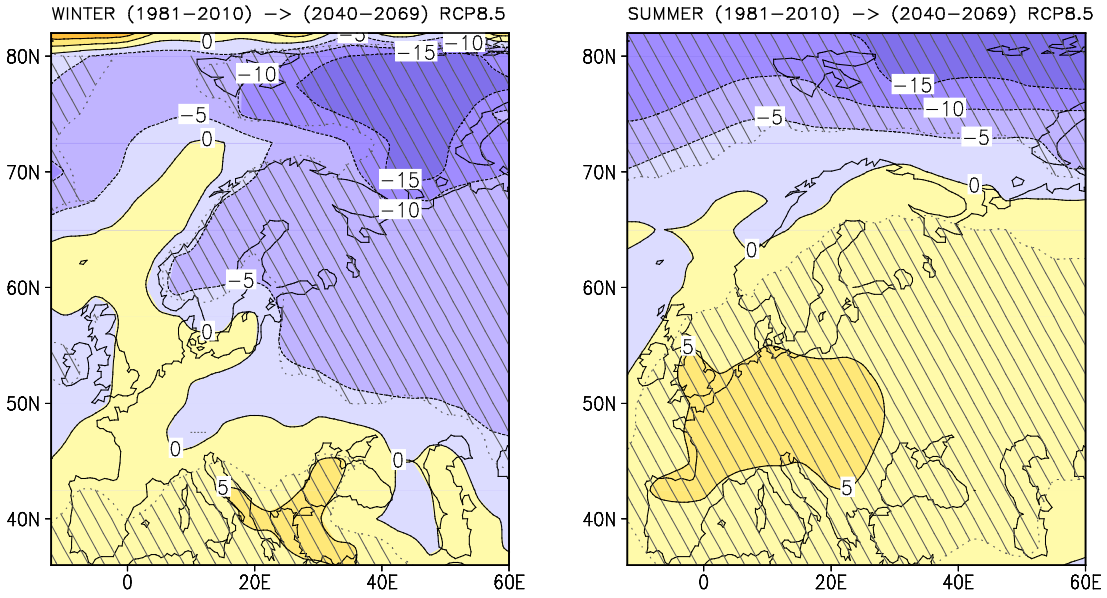

Fig. 7. Projected changes in incident solar radiation (in %) in December-February (left) and June-August (right) under the RCP8.5 scenario (see the caption of Fig. 5).

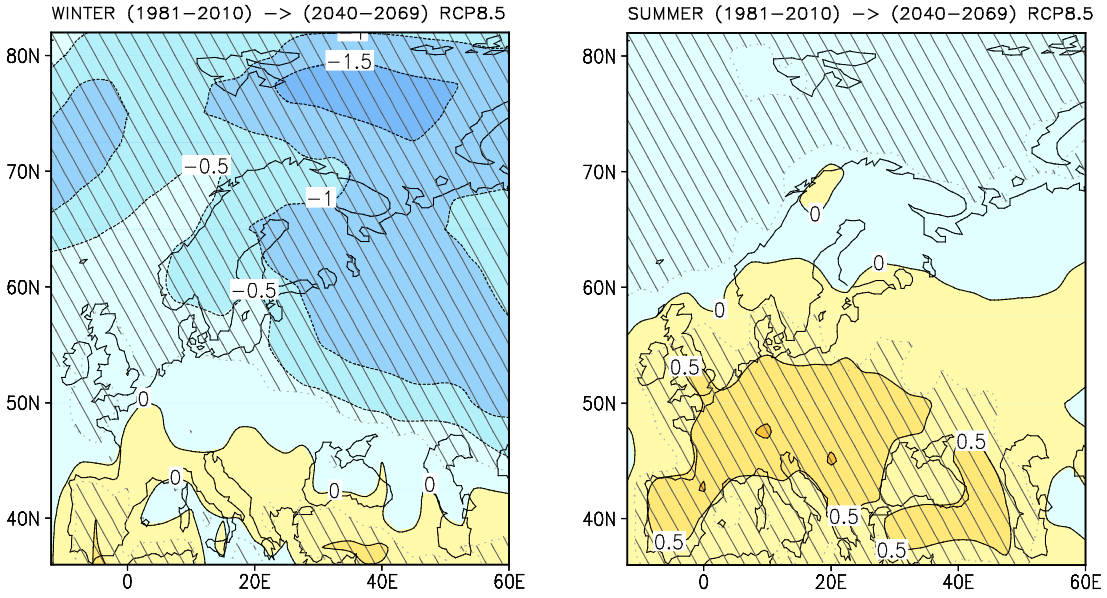

Fig. 8. Projected changes in the difference between the daily maximum and minimum temperatures (in °C) for December-February (left) and June-August (right) under the RCP8.5 scenario; an average of simulations performed with 25 GCMs (see the caption of Fig. 5).

The robustness of the multi-model mean change was assessed by studying consistency in the direction of change in the individual model projections. If more than 75 % of the 25–28 GCMs studied produced a response of the same sign, the inter-model agreement was deemed good; otherwise, we regarded the multi-model mean projection as uncertain.

Not surprisingly, the temperature response is positive and agreement among the model simulations is very high over the entire domain (Fig. 5). In winter, the most intense warming occurs over high-latitude oceans. This can be attributed primarily to the retreat of sea ice; reasons for the polar amplification of warming are discussed in more detail in section 12.4.3.1 of *IPCC* (2013). In summer, warming tends to be strong in southern Europe, which is related to decreasing precipitation totals (Fig. 6). Scantness of rain evidently cuts down soil moisture, leading to reduced evapotranspiration, and thus a larger portion of energy is transmitted into the atmosphere in the form of sensible heat. In the southernmost areas of Europe, precipitation is projected to decrease in all seasons, while north of 60°N models simulate an year-round increase. For central Europe, wetter conditions are simulated for winter and dryer for summer. In winter, the agreement in the modelled changes is generally good, apart from the zone surrounding the contour of zero change. In summer, by contrast, model-simulated precipitation projections are contradictory in large areas of central and northern Europe, including southern Finland.

Projected changes in incident solar radiation (Fig. 7) and diurnal temperature range (Fig. 8) bear many similarities in their geographical distribution. Both quantities tend to reduce in north-eastern Europe in winter and increase in central and southern Europe in summer; in these areas, model projections are concordant. Changes in both quantities are tightly linked with altering cloudiness (see Fig. 12.17 of *IPCC*, 2013). Clouds reduce incident solar radiation as well as night-time infrared cooling, both factors cutting down the differences between the day- and night-time temperatures. In part, the decrease of diurnal temperature range in the north in winter may be a reflection of reduced synoptic-scale temperature variability; this kind of reduction is clearly apparent in day-to-day temperature fluctuations (*Jylhä et al.*, 2015). During early and mid-winter in northern Europe, the regular solar-induced diurnal cycle of temperature is fairly weak.

When studying the joint distributions of modelled changes in the different climate variables across the model ensemble, striking inter-variable relationships are revealed (Fig. 9). In winter, models simulating the most intense warming for Finland likewise tend to produce the largest increases for precipitation; in the CMIP5 model ensemble, the correlation between changes in these two variables is 0.7. Such a dependence was also discovered by *Räisänen and Ylhäisi* (2015) in studying a large northern-European domain. In winter, the modelled temperature increases additionally correlate negatively with the simulated changes of incident solar radiation and diurnal temperature range. This sounds physically plausible, since in winter in high latitudes, low temperatures and large diurnal temperature variations typically occur under clear weather conditions.

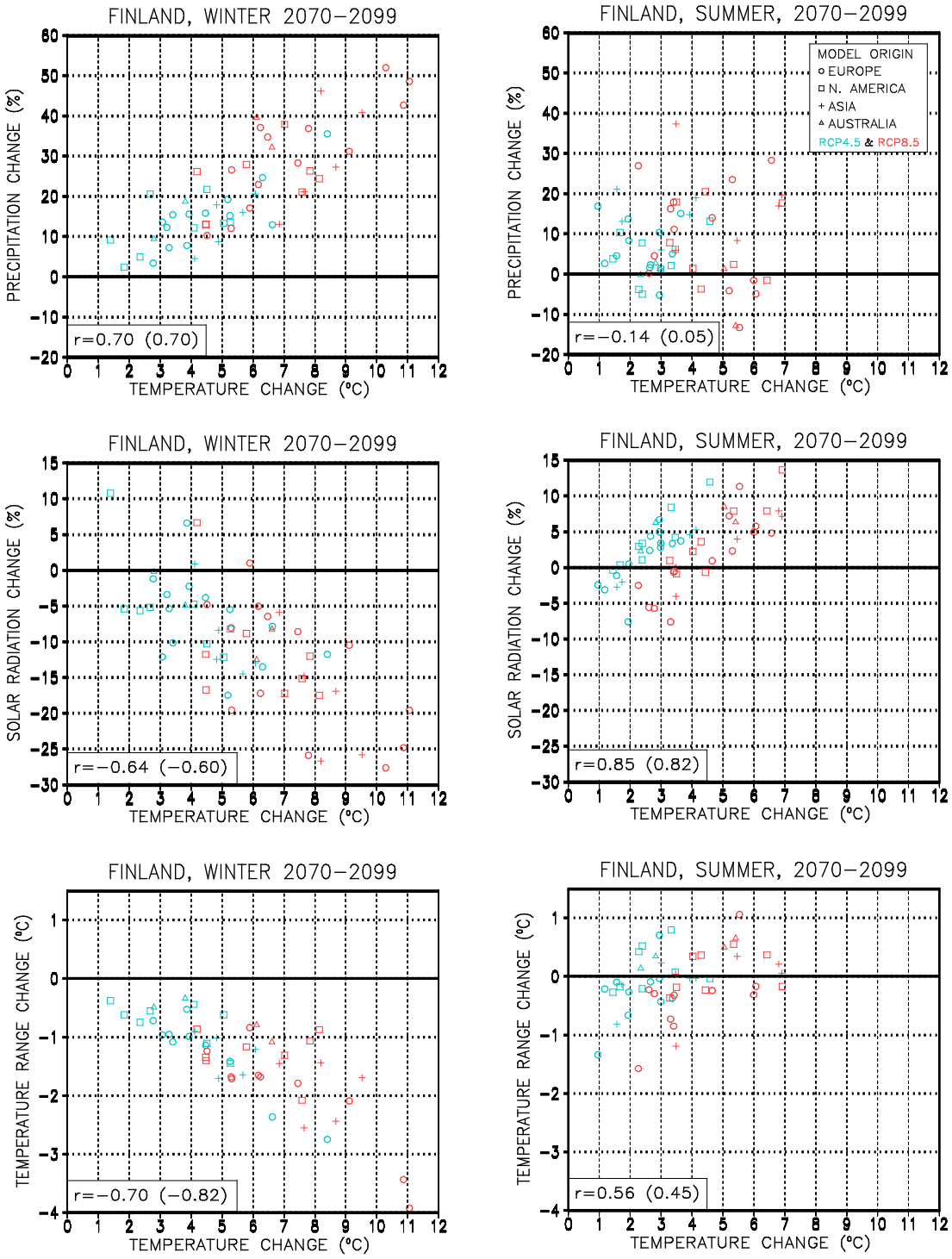

Fig. 9. Scatter diagrams showing the simulated changes (from 1981–2010 to 2070–2099) in temperature, in conjunction with changes in precipitation (top), incident solar radiation (middle) and diurnal temperature range (bottom) in Finland for the individual models. Left panels depict the bivariate distributions for December-February, right panels for June-August; model simulations under RCP4.5 have been marked by blue and those under RCP8.5 by red symbols. To facilitate the identification of the responses produced by the individual models in Tables S7–S8, models originating from different continents have been marked by distinct symbols (see the legend). The correlation coefficients between the responses in the two variables under RCP8.5 (and for RCP4.5 in parentheses) are given in the bottom-left corner of each panel. Correlations higher than 0.37 are significant at the 5 % level, those over 0.48 at the 1 % level (when data are available from 28 GCMs, implying $df = 26$).

In summer, there is little dependence between the temperature and precipitation responses, but the magnitude of warming correlates positively with changes in solar radiation and diurnal temperature range (Fig. 9, right panel). In particular, these relationships are apparent when studying the two RCP scenarios separately. The interpretation of these findings is straightforward. In summer when solar radiation is strong, the magnitude of warming depends both on the strength of greenhouse gas forcing and changes in cloudiness, the latter determining changes that take place in incident solar radiation. In all models, greenhouse gas forcing itself leads to a stronger warming under RCP8.5 than under RCP4.5. Under both scenarios, this warming is amplified or attenuated by changes in the heat provided in the form of solar radiation. Accordingly, for a specified temperature increase, the responses in incident radiation are systematically smaller under RCP8.5 than under RCP4.5. An additional factor that may contribute to these systematic inter-scenario differences is the somewhat stronger aerosol dimming under RCP8.5. Increasing solar radiation likewise acts to enhance diurnal temperature variations; this explains the positive correlation between changes in the mean temperature and its diurnal range.

Furthermore, we found a statistically significant negative inter-model correlation between changes in surface pressure and precipitation (not shown). This relationship, also reported by *Räisänen and Ylhäisi* (2015), evidently reflects the well-known connection between cyclonic activity and precipitation.

3.2 Contribution of modelling differences and internal variability to the projection uncertainty

The temporal evolution of the total uncertainty (in the form of standard deviation) in climate projections for Finland under RCP4.5, along with the contributions of inter-model differences and internal variability, is shown in Fig. 10. As discussed in section 2.3, the standard deviation describing the component due to internal variability is approximated here by a constant value. Three variables are examined: mean temperature, precipitation and incident solar radiation.

For temperature and solar radiation, uncertainty in the projected changes is mainly explained by modelling differences, apart from the first decades (Fig. 10). Conversely, in the precipitation projections the influence of internal variability dominates throughout the century.

For RCP8.5 (Fig. S12), the behaviour of uncertainty in temperature and solar radiation is qualitatively similar to that under RCP4.5, although both the multi-model mean response itself and the projection uncertainty are increasing more rapidly in time. For precipitation, the contribution of inter-model differences likewise exceeds the component due to internal variability from the 2050s onwards. Note also that partitioning of the uncertainty variance for precipitation failed during the first few decades of the century. Reasons for that failure are discussed at the end of section A2 in the Appendix.

The present findings are in line with *Ylhäisi et al.* (2015) who likewise reported a substantially larger importance of internal variability in the uncertainty of precipitation than temperature projections.

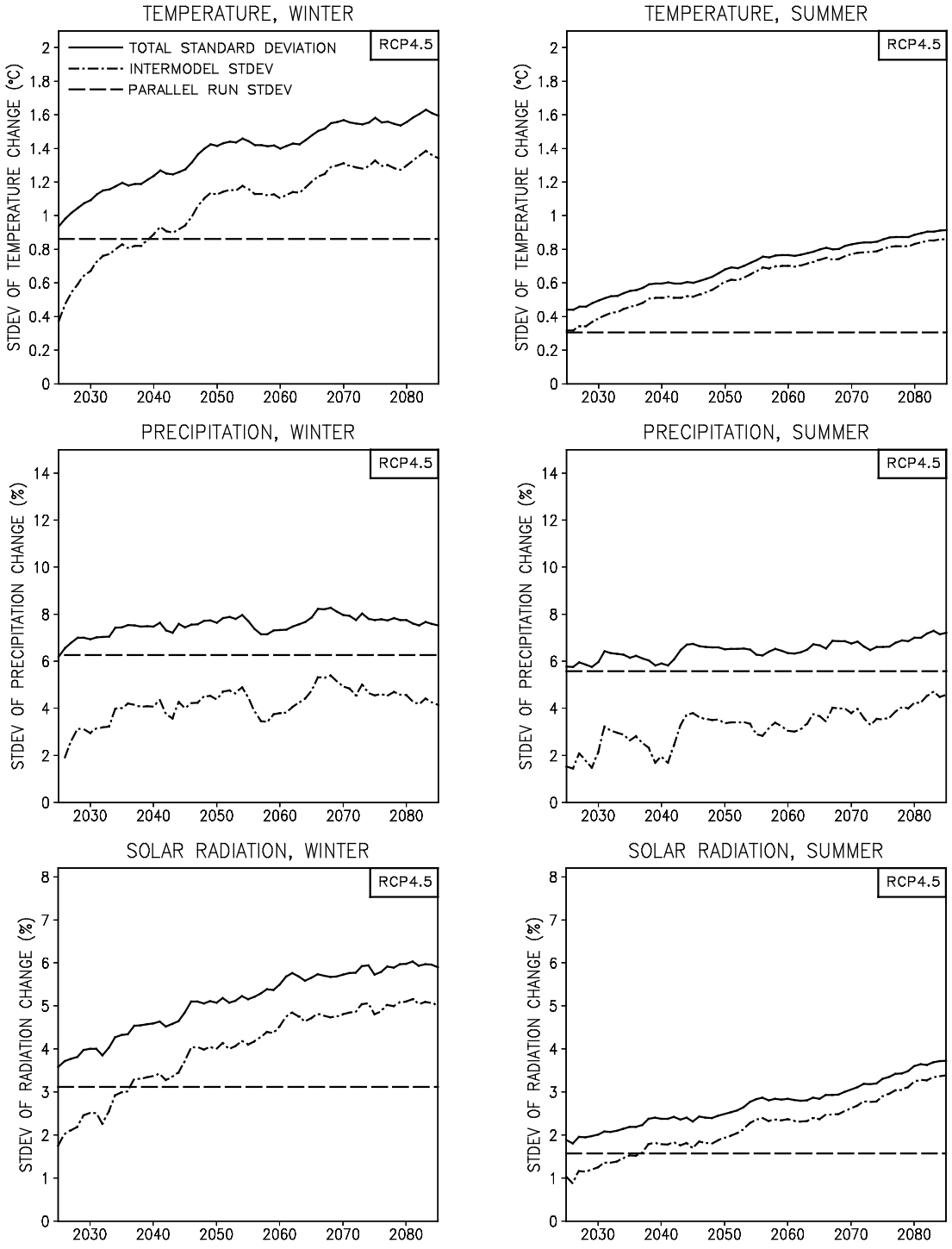

Fig. 10. Temporal evolution of the standard deviation describing uncertainty in the 30-year running mean change in mean temperature (in °C, top), precipitation (in %, middle) and incident solar radiation (in %, bottom) in Finland under the RCP4.5 scenario. Left panels show the uncertainties for December-February, right panels for June-August. The total uncertainty (solid curves) has been decomposed into contributions arising from the true inter-model differences (dash-dotted curves) and differences between the parallel runs (dashed horizontal line); the latter serves as an estimate for internal variability.

3.3 Comparison to the projections derived from CMIP3 GCMs

In *Jylhä et al.* (2009), future projections of temperature and precipitation for Finland were given under three SRES scenarios. As discussed in section 2.1, in the old SRES B1 and the new RCP4.5 scenario the future evolution of radiative forcing is very similar. This permits a quantitative intercomparison of the resulting projections. As an exception to the convention followed elsewhere in this paper, in this comparison we have employed the same reference period as in *Jylhä et al.* (2009), 1971–2000.

The seasonal cycle of the projected temperature and precipitation changes in Finland, as derived from both model ensembles, is presented in Fig. 11. The multi-model mean precipitation projections produced by the two model generations are surprisingly identical throughout the year (Fig. 11, right panel). The temperature projections (left panel) are likewise fairly similar from November to March, but for the rest of the year the new CMIP5 models tend to yield stronger warming, with the inter-ensemble difference being largest in August, about 1°C. Nevertheless, compared to the fairly wide uncertainty intervals of the projection, the difference between the model generations is not very impressive.

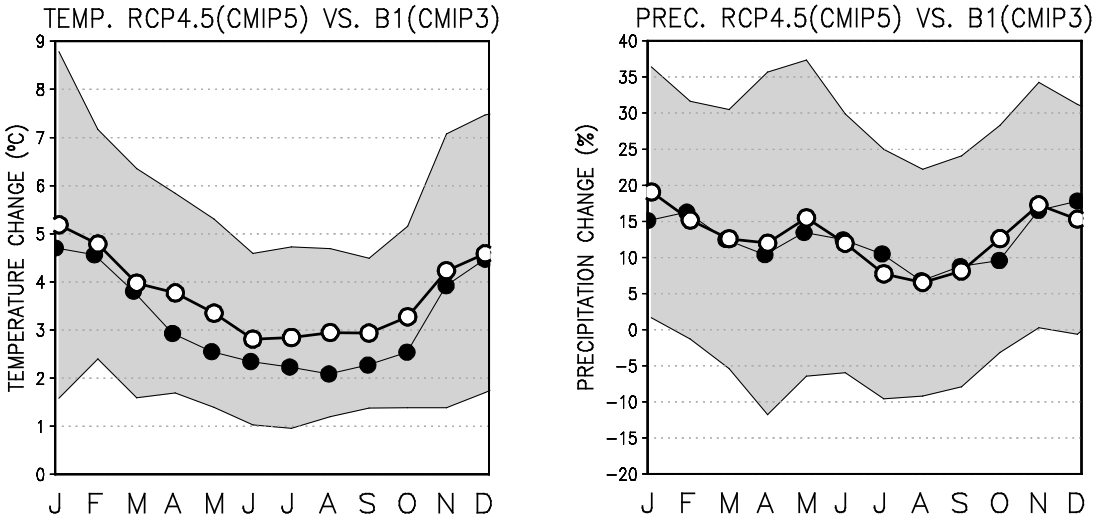

Fig. 11. Projected changes in mean temperature (in °C, on the left) and precipitation (in %, on the right) in Finland for the period 2070–2099, relative to 1971–2000; a comparison between the new CMIP5 and old CMIP3 simulations. The multi-model mean projections for individual calendar months (J = January, F = February, ...) are given for the SRES B1 scenario (19 CMIP3 GCMs; closed circles) and for RCP4.5 (28 CMIP5 GCMs; open circles). In addition, the 90 % uncertainty intervals for the change (analogous to those depicted in Figs. 3 and 4) are given for RCP4.5 (grey shading).

The present analysis of CMIP5 vs. CMIP3 differences can be compared with an analogous exercise by *Räisänen and Ylhäisi* (2015), but it should be noted that the analyses are not entirely commensurable. Firstly, *Räisänen and Ylhäisi* (2015) studied spatial averages over a wide northern European domain rather than merely Finland. Secondly, in that research an identical forcing was employed for both model ensembles: an 1 % annual increase in the atmospheric concentration of carbon dioxide. This allowed

Räisänen and Ylhäisi (2015) to isolate the influence of disparity in the model ensembles, whereas our comparison is affected, to some extent, by the update of greenhouse gas scenarios.

In spite of these methodological differences, the behaviour of the temperature response in Fig. 11 is well in accord with *Räisänen and Ylhäisi* (2015), who likewise found a larger summertime temperature increase for the CMIP5 than for the CMIP3 GCMs. Conversely, we did not find any signal of a smaller increase in the annual precipitation total in CMIP5, as reported by *Räisänen and Ylhäisi* (2015) for the larger northern European domain.

CMIP3-based projections for incident solar radiation over Europe and the northern Atlantic have been produced by *Ruosteenoja and Räisänen* (2013). The geographical distributions of the seasonal changes (Fig. 2 of *Ruosteenoja and Räisänen*, 2013) were broadly similar to those presented in Fig. S9. In summer, an increase in solar radiation was projected nearly for the entire European continent, with a maximum over western and central Europe. In winter, by contrast, some dissimilarities occur: according to the CMIP3 simulations, the contour of zero change resided close to 45°N, whereas in the present projections a slight increase is simulated for some areas of north-western Europe. Even so, both model ensembles produced the largest decreases for the Barents Sea area and northeastern Europe and increases for south-eastern Europe.

By studying a set of nine CMIP3 GCMs, *Gregow et al.* (2012) reported a small increase of 2–4 % in mean geostrophic wind speeds for the period 2081–2100 for southern Finland in autumn and in winter. Conversely, in the present analysis the monthly-mean true wind speeds derived from CMIP5 did not reveal any notable multi-model mean change, even though the inter-model spread in the projections was substantial (Figs. 3–4). *Räisänen and Ylhäisi* (2015) reported a substantially smaller increase in the westerly component of the time-mean geostrophic wind in northern Europe in the CMIP5 than in the CMIP3 ensemble (see their Fig. 3); evidently, this is related to the absence of mean wind speed intensification in the CMIP5 ensemble.

3.4 Downscaled simulations

The monthly mean temperature, precipitation and incident solar radiation responses for Finland simulated by nine driving GCMs (section 2.2, Table 1), along with the corresponding downscaled simulations produced by the RCA4 RCM, are presented in Fig. 12. To make the RCM and GCM responses strictly comparable, for each GCM only the single parallel run equivalent to the RCM simulation was included in the analysis. We concentrate on the late-century 30-year period during which the climate change signal is most robust and, consequently, the differences between the RCM and GCM simulations are most readily noticeable.

Regarding the means of the nine model simulations, dynamical downscaling tends to enhance the seasonal contrast of warming. In the RCM simulations, on average, the projected temperature increase is stronger in winter and weaker in summer compared to the corresponding sub-ensemble of GCM runs (Fig. 12). Increases in precipitation are more ample throughout the year. A similar disparity in the temperature and precipitation

projections is also apparent in the GCM/RCM comparison conducted for Sweden (*Strandberg et al.*, 2014, the participating models were the same as in the present study). Furthermore, the RCM ensemble projects less solar radiation than the corresponding GCM ensemble (Fig. 12). In summer, the multi-model mean radiation responses derived from the two model categories are even of opposite sign. In winter, the RCM simulations yield a stronger reduction in radiation. All the above-mentioned features are evident under RCP4.5 as well, albeit the differences are smaller in quantitative terms (Fig. S13).

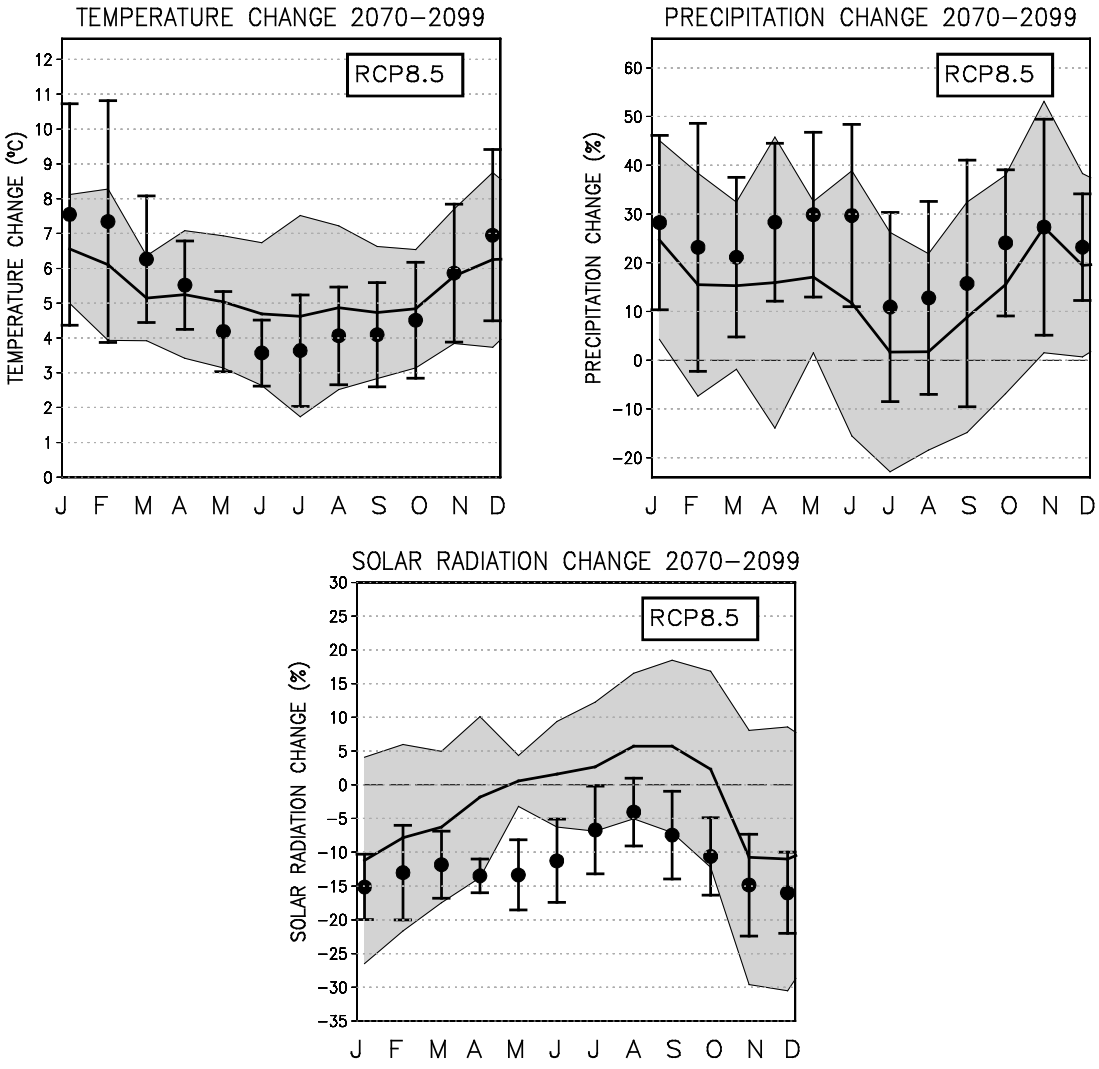

Fig. 12. Monthly-mean changes in temperature (in °C, top left), precipitation (in %, top right) and incident solar radiation (in %, bottom) in Finland for the period 2070–2099 (relative to 1981–2010) under RCP8.5 as inferred from nine driving GCMs and from the corresponding simulations downscaled by the RCA4 regional model. The mean of the projections produced by the driving GCMs has been denoted by a thick curve, grey shading showing the 90 % uncertainty interval for the GCM-derived change. The average of the RCM responses has been denoted by bullets and the corresponding uncertainty intervals by vertical bars.

In a physical sense, the RCM versus GCM differences in the projected changes appear consistent. The strong decrease in insolation projected by the RCM is evidently an indication of a substantial increase in cloudiness, and cloudy sky is typically associated with mild weather in winter and cool conditions in summer, favouring the occurrence of precipitation in all seasons.

The uncertainty ranges of the projected changes tend to become narrower when derived from the RCM runs than from the nine driving GCM simulations (Fig. 12). This particularly holds for radiation and, in April through September, also for temperature. For precipitation year-round and temperatures in October to March, by contrast, the uncertainty intervals are of a similar order of magnitude or, in some cases, even larger when derived from the RCM simulations. One explanation for this finding might be the substantial contribution of internal variability to the precipitation and winter temperature projections, while in the uncertainty of the insolation and summer temperature responses, inter-model differences dominate (Figs. 10 and S12). As a caveat, it should be stated that the present uncertainty intervals are less robust than those depicted in Figs. 3–4, since the number of models is now smaller and only one parallel run per model is available. The absence of multiple parallel runs likewise inhibits any effort to decompose the RCM-produced uncertainty variances.

The tendency towards narrower projection uncertainty intervals indicates that the RCA4 model does not merely act as a microscope that generates fine-scale features into the GCM-simulated climate response. Rather, RCA4 tends to create its own regional climate that is partially independent of the driving GCM. This property is most evident in summer. In winter, in contrast, atmospheric circulation is strong, and the influence of boundary data adopted from the driving GCM is more effectively advected into Finland that is located in the central areas of the RCM domain.

In spite of the finer computational grid, the baseline-period climate in the RCA4 RCM is in many respects even more biased than in the driving GCMs. In particular, temperatures simulated for Finland are 2–3 degrees colder than those observed and, consequently, less consistent with the observations than in the simulations of the nine GCMs on average (*Strandberg et al.*, 2014). The driving GCMs likewise outperform RCA4 in the simulation of summer precipitation. On the other hand, regional models can resolve the climatic influence of the distribution of land and sea and orography more accurately than GCMs. Therefore, the added value provided by spatial downscaling is most pronounced in areas with highly varying topography. Also, the fine resolution employed in RCMs allows to simulate diverse small-scale weather phenomena that remain unresolved in GCMs. This makes RCMs a suitable tool for studying small-scale climate extremes, such as events of heavy precipitation (*Jacob et al.*, 2014).

4 Discussion

Although the projected trend towards warmer and, in winter, wetter conditions is unequivocal, there is still quite a large quantitative uncertainty in the forecasted changes. In the present work, we have focussed on those two components of uncertainty that

are independent of human behaviour and climate policy: modelling differences and internal variability. In contrast, it is much more difficult to find any objective method to attach probabilities to the four RCP forcing scenarios. In fact, it is very likely that none of them will be realized as such. For example, the climatic response to the high-emission RCP8.5 scenario is so extreme that a collapse of human civilization would evidently ensue far before the year 2100. Such a global catastrophe would curtail anthropogenic greenhouse gas emissions drastically.

As an example of a different approach, *Ylhäisi et al.* (2015) decomposed the variance describing projection uncertainty into three components, with the forcing scenario uncertainty covering the entire range of greenhouse gas concentration pathways from RCP2.6 to RCP8.5; all four RCP scenarios were regarded as equally plausible. Considering the seasonal temperature projections for the Nordic area by the late 21st century, inter-model differences proved to account for about 60–70 % and greenhouse gas scenario differences 20–40 % of the total uncertainty variance, while the contribution of internal variability was negligible. Conversely, for the precipitation projections, the uncertainty due to the diverging forcing scenarios was smaller than that originating from internal variability (apart from winter).

In our analyses, seven CMIP5 GCMs with a very low performance were excluded (section 2.2). For sensitivity assessment, we re-calculated the temperature and precipitation projections by including all 35 models. The multi-model mean responses proved to be very similar to those based on the manifold of 28 GCMs, but the resulting uncertainty intervals were somewhat wider. This was primarily caused by the inclusion of the FIO-ESM model which simulated responses that deviated strongly from the remaining GCM simulations (see Fig. 12.9 of *IPCC*, 2013). That model was likewise rejected in several analyses incorporated in the IPCC report.

In addition to the six climate quantities explored in the present paper, we have looked at relative air humidity, but for that variable the quality of model data proved to be mixed. For example, several models simulated physically unfeasible humidities higher than 100 % for the cold season, and the future trends modelled for relative humidity contradicted those for the other variables. For readers interested in the projections of relative humidity, we refer to our former calculations based on the CMIP3 models (*Ruosteenoja and Räisänen*, 2013; *Ruosteenoja et al.*, 2013). Considering the reasonable agreement between the projections derived from the two model generations for the other quantities (section 3.3), those humidity projections are likely to be still valid, at least qualitatively.

No GCM (or RCM) can simulate the observed climate accurately but some modelling biases always occur. Therefore, in framing estimates for future monthly mean temperature, precipitation, etc., modelled values must never be applied as such. For example, if the model-simulated baseline-period mean temperature were 4°C below that observed and the temperature increase obtained for some future period were 3°C, the modelled mean temperature for that future span would still be 1°C below that observed during the baseline period! Instead, one should apply the delta-change approach, in which the model-projected monthly or seasonal mean temperature increase is added di-

rectly to the corresponding observational temperature. Analogously, future precipitation totals are found by multiplying the observed mean precipitation by the factor $1 + \Delta P/100$, where ΔP is the modelled precipitation change expressed in per cent. More detailed guidance on the use of the delta-change approach is given in *Jylhä et al.* (2004) and references therein.

An alternative, widely-used technique for creating forecasts for mean temperatures and other climate variables for the future is termed bias correction. This method consists of modifying the model output for the baseline period to be consistent with observations (e.g, by adjusting the temporal means and standard deviations) and then applying the resulting correction factors to the simulated future climate. Bias correction has been applied widely for RCM data (e.g., *Räisänen and Räty*, 2013, and references therein) but also for GCM output (e.g., *Ruosteenoja et al.*, 2015). Various bias correction methods have been discussed in *Räisänen and Räty* (2013).

5 Conclusions

As a consequence of global warming, substantial changes will take place in the Finnish climate. The projected changes are most prominent in winter: mean surface air temperature is estimated to rise 1.6–1.7 times as much as in summer, precipitation may increase by several tens of percent by the end of this century and incident solar radiation and diurnal temperature range are expected to diminish remarkably. In summer, mean temperature is projected to rise as well, albeit not as much as in winter. For summer precipitation, solar radiation and diurnal temperature range, even the sign of the change is uncertain, although a majority of GCMs simulate increases both for precipitation and solar radiation.

When studying the changes simulated by the individual GCMs, projections for the various climate quantities proved to behave consistently. In winter, the fundamental climate change signal is constituted by an increase in temperature and precipitation and an attenuation in the diurnal temperature cycle and solar radiation. Multivariate distributions of the projected changes (Fig. 9) revealed that this signal was produced by a vast majority of the models, but the response manifested itself in a varying amplitude in the different models. In summer, by contrast, there was little relationship between the projected changes of temperature and precipitation. Even so, models with the largest projected warming tended to increase insolation and diurnal temperature range most vigorously.

Although the inter-model agreement on the sign of the response was good over large areas or, for temperature, even for the whole Europe, uncertainty intervals in the projected changes were broad. For example, if the RCP8.5 scenario were realized, mid-winter temperatures in Finland would increase by 2–7°C and precipitation by 3–36 % by the mid-21st century (Fig. 3). For temperature and solar radiation, the uncertainty in the projection mostly reflected modelling differences, while for precipitation, the contribution of internal variability was prominent.

Global warming does not necessarily alter all the characteristics of climate. For example, the multi-model mean change in wind speed for Finland was nearly zero throughout the year. Still, individual model projections for this quantity were contradictory and the uncertainty intervals wide.

Compared with the large differences amongst the individual model projections, differences between the multi-model means derived from the present and the previous model generations were rather modest (section 3.3). A similar conclusion was drawn by *Räisänen and Ylhäisi* (2015), who present two alternative interpretations for this finding: either the models are already qualified enough so that no significant progress is possible any more; or no radical improvement in modelling has taken place since the publication of the previous model generation. The latter, less fascinating inference is supported by the large divergence among the model simulations that has not narrowed remarkably between the generations. Certainly, the count of GCMs is larger in the CMIP5 ensemble, which allows inferring more robust uncertainty estimates.

In the present work, only the long-term climatological means were examined. Simulations of diverse extreme events, such as heavy rains, may still benefit from the finer horizontal and vertical resolution in the new-generation models.

For a sub-ensemble of nine GCMs, we analyzed simulations downscaled dynamically by the RCA4 RCM. Remarkable differences were revealed in the responses produced for Finland by the driving GCMs and this particular RCM. For example, the RCM projections were wetter, with larger increases in precipitation and reduction in insolation compared to the projections directly based on the driving GCMs. Moreover, downscaling tended to considerably suppress inter-model differences in the projected changes of solar radiation and (apart from the cold season) temperature. Accordingly, we do not recommend the present manifold of RCM simulations to be used in compiling mean temperature, precipitation etc. projections for climate change adaptation studies; rather, the GCM-derived projections should be preferred. This particularly holds for such research subjects for which reliable uncertainty estimates are essential.

As a continuation to the present work, we plan to extend the analyses into new climate variables, such as soil moisture, snow water equivalent and the components of geostrophic wind. Additionally, inter-variable dependencies may be examined more comprehensively than we did in section 3.1.

To conclude, there is still a substantial scatter among the model projections. Moreover, the climatic conditions that will prevail during the late 21st century depend much on the future evolution of greenhouse gas emissions. All decisions concerning adaptation to changing climate have thus to be grounded on uncertain quantitative information. Nevertheless, the general tendency towards warmer and, in winter, wetter climate in Finland is highly evident.

Acknowledgements

This work has been funded by the SETUILMU research activity of the Advisory Board for Sectoral Research (via the SETUKLIM project) and by the Academy of Fin-

land (the PLUMES and ADAPT projects, decisions 278067 and 260785). The CMIP5 GCM data were downloaded from the EARTH System Grid Federation data archive (http://pcmdi9.llnl.gov) and RCA4 simulations from the Swedish Meteorological and Hydrological Institute (bi.nsc.liu.se). Tiina Ervasti and Jouni Räisänen are acknowledged for useful comments.

Supporting information

This paper is accompanied by a supplement file that provides information about the projected seasonal changes of six climate variables (mean temperature, precipitation, surface pressure, incident solar radiation, diurnal temperature range and scalar wind speed); both the multi-model statistics (Tables S1–S6) and changes simulated by the individual GCMs (Tables S7 and S8). The projected monthly multi-model mean changes and uncertainty intervals for these variables under RCP4.5 are presented in Figs. S1–S3 (a similar representation as in Figs. 3–4). The geographical distributions of the multi-model mean changes of four climate quantities for the periods 2020–2049 and 2070–2099 are shown in Figs. S4–S11 (to be compared with the estimates for the period 2040–2069, presented in Figs. 5–8). Figure S12 depicts the components of uncertainty under RCP8.5, analogously to Fig. 10. A comparison of changes produced by nine driving GCMs to the corresponding dynamically downscaled responses under RCP4.5 are given in Fig. S13 (analogous to Fig. 12 that deals with the RCP8.5 scenario). Finally, Fig. S14 shows GCM-derived estimates for the temperature sum of the thermal growing season for three tridecadal periods (data extracted from *Ruosteenoja et al.*, 2015).

Appendix: Technical details of processing the model output data

A1. Pattern scaling

For the RCP2.6 and RCP6.0 scenarios, data are lacking from a substantial portion of the GCMs (Table 1). If the multi-model mean responses were calculated directly from the GCM simulations available for each particular RCP scenario, the set of models would be different for the various forcing scenarios, and thereby the resulting multi-model means would not be commensurable. To resolve this problem, surrogate data need to be generated for the missing model runs.

Surrogate data were created by employing a modified version of the super-ensemble pattern-scaling technique introduced in *Ruosteenoja et al.* (2007). In this approach, it is assumed that the local or regional-scale change in any arbitrary climate variable is proportional to the global mean temperature change:

$$\Delta X^{*}_{sm} = a_{xm} \left\langle \Delta T_s \right\rangle \tag{1}$$

where $\left\langle \Delta T \right\rangle$ is the global mean temperature change and ΔX^{*} the resulting estimate for regional change in the climate variable X (e.g., the spatial mean of temperature or precipitation over Finland) for model m. The subindex s refers to the RCP scenario for which surrogate data are created (in this case, RCP2.6 or RCP6.0) and

$$a_{xm} = \frac{\sum_{s=1}^{S_m} \left\langle \Delta T_s \right\rangle \Delta X_{sm}}{\sum_{s=1}^{S_m} \left\langle \Delta T_s \right\rangle^2} \tag{2}$$

is a least-square regression line that is constrained to pass through the origin. ΔX stands for the GCM-simulated change in X and S_m for the number of RCP scenarios for which runs are available for climate model m. For models with multiple parallel runs available for a RCP scenario, ΔX represents their mean.

In *Ruosteenoja et al.* (2007), global mean temperature responses $\left\langle \Delta T_s \right\rangle$ to the different greenhouse gas scenarios were calculated by using a simple energy balance climate model. In the present work, a different approach was applied. For the models with simulations for one or two RCP scenarios lacking, we assumed that the ratios of $\left\langle \Delta T_{sm} \right\rangle$ between the various RCP scenarios would be similar to those in the remaining models on average. For that purpose, we first sought for the medians for the ratios $\left\langle \Delta T_{sm} \right\rangle / \left\langle \Delta T_{RCP4.5,m} \right\rangle$ within the model ensemble (s represents either RCP2.6, 6.0 or 8.5; all values of $\left\langle \Delta T_{sm} \right\rangle$ are means over parallel runs). After that, we determined the median of $\left\langle \Delta T_{RCP4.5,m} \right\rangle$ from the set of 28 models. By multiplying these medians, we obtained a multimodel estimate for $\left\langle \Delta T_s \right\rangle$ for the three remaining RCP scenarios. Multimodel medians rather than means were used to suppress the impact of outliers, i.e., models simulating global mean changes deviating substantially from those in the majority of the

GCMs. By inspecting Eqs. (1)–(2), one can see that it is not the absolute values of $\langle \Delta T_s \rangle$ but the ratios of $\langle \Delta T_s \rangle$ among the various scenarios that basically determine the regression coefficient *a* and thereby the scaled values of ΔX.

It should be emphasized that scaling does not have any impact on the projections for RCP4.5 and RCP8.5 but only those under the RCP2.6 and RCP6.0 scenarios.

A2. Partition of the uncertainty variance

This section summarizes the discussion presented in sections 2.3 and S1 of *Ruosteenoja et al.* (2015).

Basically, the uncertainty of future changes in any climate variable consists of three components: (i) the unforeseeable future evolution of the abundance of greenhouse gases, (ii) modelling uncertainty (approximated here by the differences among responses produced by the available models) and (iii) internal natural variability. Component (i) is not studied explicitly, since we present results for the various RCP scenarios separately. For components (ii)–(iii), their contributions to uncertainty can be assessed by exploring the entire set of simulations performed with the 28 GCMs (Table 1).

Considering all GCMs we have, besides the first run for every GCM, in total 36 (RCP4.5) or 32 (RCP8.5) additional parallel runs.

Ensemble means of the projected change for every model can be calculated by

$$\overline{\Delta X}_m = \frac{1}{N_m} \sum_{i=1}^{N_m} \Delta X_{im} \tag{3}$$

where N_m is the number of parallel simulations for model *m* under the RCP scenario inspected. ΔX_{im} stands for the modelled change in the climate variable (e.g., temperature or precipitation) from 1981–2010 to the tridecadal scenario period in the parallel run *i*.

The number of parallel runs per model and RCP scenario varies from 1 to 6 (Table 1). Such a small count is far from sufficient for inferring reliable estimates of internal variability by studying each individual model separately. However, if we assume that the magnitude of internal variability is similar for all models (this approximation was likewise employed in (15) of *Yip et al.* (2011)), the resulting contribution to the uncertainty variance σ_{int}^2 can be estimated by treating the deviations of individual parallel runs under the specific RCP scenario from the corresponding ensemble mean as a single sample:

$$\sigma_{\text{int}}^2 = \frac{\Sigma_{m=1}^{M} \Sigma_{i=1}^{N_m} \left(\Delta X_{im} - \overline{\Delta X}_m \right)^2}{\Sigma_{m=1}^{M} N_m - M} \tag{4}$$

where *M* is the total number of models. It appeared that there was no trend in σ_{int}^2, provided that the baseline and scenario periods did not overlap or be very close to one an-

other, but the temporal variations of that quantity were fairly noisy. To enhance the robustness of the estimate (4), we averaged σ^2_{int} over all four RCP scenarios and over the period 2040–2099 and used this constant value of σ^2_{int} in the ensuing decomposition (7).

The variance related to the true inter-model differences can be expressed in the form (for derivation, see section S1 in the supplement file of *Ruosteenoja et al.*, 2015):

$$\sigma^2_{gcm} = D^2\left(\overline{\Delta X}_m\right) - \frac{\sigma^2_{\text{int}}}{N_{eff}} \tag{5}$$

where $D^2\left(\overline{\Delta X}_m\right)$ is the inter-model variance of the parallel-run means and the effective number of parallel runs per model is given by

$$N_{eff} = \left(\frac{1}{M}\sum_{m=1}^{M}\frac{1}{N_m}\right)^{-1} \tag{6}$$

For variables with data available from all 28 GCMs (e.g., temperature and precipitation), the value of N_{eff} was 1.42 for RCP4.5 and 1.36 for RCP8.5.

Using the available GCM data, we can readily calculate $D^2(\overline{\Delta X}_m)$ and σ^2_{int}. Thereby, an estimate for the contribution of the true model differences is obtained by Eq. (5). Finally, the total variance of uncertainty is given by the sum of Eqs. (4) and (5):

$$\sigma^2_{tot} = \sigma^2_{gcm} + \sigma^2_{\text{int}} = D^2\left(\overline{\Delta X}_m\right) + \sigma^2_{\text{int}}\frac{N_{eff}-1}{N_{eff}} \tag{7}$$

The decomposition (7) was only calculated for those two forcing scenarios (RCP4.5 and RCP8.5) for which we had data from every GCM. Calculation of N_{eff} by Eq. (6) would not be possible for RCP2.6 and RCP6.0 since simulations are lacking from some models (yielding $N_m = 0$ in the denominator of Eq. (6) for those models). In this case, use of pattern-scaled surrogate values would not be reasonable, since these are not statistically independent but derived from simulations performed under the other RCP scenarios (section A1).

Finally, a caveat should be mentioned: if the amplitude of internal variability differs substantially across the models, the above-presented estimates may become biased. Namely, in calculating σ^2_{int} by Eq. (4), one gives an enhanced weight to those models that provide numerous parallel simulations. Conversely, in Eq. (5) this kind of weighting is not applied.

In some special cases, the above-mentioned bias phenomenon or sampling variability caused by the limited number of models may lead to a situation in which the estimated total uncertainty variance is smaller than the approximation calculated for internal variability; this yields an imaginary value for the calculated inter-model standard

deviation. An example of this kind of situation is seen in Fig. S12, in which the partition of the uncertainty variance of precipitation failed before about 2040.

References

Aalto, J., P. Pirinen and K. Jylhä, 2016. New gridded daily climatology of Finland — Permutation-based uncertainty estimates and temporal trends in climate. *Journal of Geophysical Research — Atmospheres*, doi:10.1002/2015JD024651.

Carter, T.R., M. Posch and H. Tuomenvirta, 1996. The SILMU scenarios: specifying Finland's future climate for use in impact assessment. *Geophysica*, **32**, 235–260.

Carter, T.R., K. Jylhä, A. Perrels, S. Fronzek and S. Kankaanpää, 2005. FINADAPT scenarios for the 21st century — Alternative futures for considering adaptation to climate change in Finland. No. 332 in Mimeographs, Finnish Environment Institute, Helsinki, Finland. FINADAPT working paper 2.

Carter, T.R., S. Fronzek, A. Inkinen, I. Lahtinen, M. Lahtinen, H. Mela, K.L. O'Brien, L.D. Rosentrater, R. Ruuhela, L. Simonsson and E. Terama, 2014. Characterising vulnerability of the elderly to climate change in the Nordic region. *Regional Environmental Change*, doi:10.1007/s10113-014-0688-7.

Fortelius, C., E. Holopainen, J. Kaurola, K. Ruosteenoja and J. Räisänen, 1996. Climate models and scenarios. In: J. Roos (Ed.), The Finnish Research Programme on Climate Change (SILMU), Final Report, vol. 4/96, 43–49, Publications of the Academy of Finland.

Gong, J., S. Kellomäki, K. Wang, C. Zhang, N. Shurpali and P.J. Martikainen, 2013. Modeling CO_2 and CH4 flux changes in pristine peatlands of Finland under changing climate conditions. *Ecological Modelling*, **263**, 64–80, doi:10.1016/j.ecolmodel.2013.04.018.

Gregow, H., K. Ruosteenoja, N. Pimenoff and K. Jylhä, 2012. Changes in the mean and extreme geostrophic wind speeds in Northern Europe until 2100 based on nine global climate models. *International Journal of Climatology*, **32**, 1834–1846, doi:10.1002/joc.2398.

Huttunen, I., H. Lehtonen, M. Huttunen, V. Piirainen, M. Korppoo, N. Veijalainen, M. Viitasalo and B. Vehviläinen, 2015. Effects of climate change and agricultural adaptation on nutrient loading from Finnish catchments to the Baltic Sea. *Science of the Total Environment*, **529**, 168–181, doi:10.1016/j.scitotenv.2015.05.055.

IPCC, 2007. Climate Change 2007: The physical science basis. Contribution of Working Group I to the Fourth Assessment Report of the Intergovernmental Panel on Climate Change. Cambridge University Press, Cambridge, U.K., 996 pp. [S. Solomon, D. Qin, M. Manning, Z. Chen, M. Marquis, K. B. Averyt, M. Tignor and H. L. Miller (eds.)].

IPCC, 2013. Climate Change 2013: The physical science basis. Contribution of Working Group I to the Fifth Assessment Report of the Intergovernmental Panel on Climate Change. Cambridge University Press, Cambridge, U.K., 1535 pp. [Stocker, T.F., D. Qin, G.-K. Plattner, M. Tignor, S.K. Allen, J. Boschung, A. Nauels, Y. Xia, V. Bex and P.M. Midgley (eds.)].

Irannezhad, M., D. Chen and B. Kløve, 2015. Interannual variations and trends in surface air temperature in Finland in relation to atmospheric circulation patterns, 1961–2011. *International Journal of Climatology*, **35**, 3078–3092, doi:10.1002/joc.4193.

Jaagus, J. and K. Mändla, 2014. Climate change scenarios for Estonia based on climate models from the IPCC Fourth Assessment Report. *Estonian Journal of Earth Sciences*, **63**, 166–180, doi:10.3176/earth.2014.15.

Jacob, D., J. Petersen, B. Eggert, A. Alias, O. B. Christensen, L. Bouwer, A. Braun, A. Colette, M. Déqué, G. Georgievski, E. Georgopoulou, A. Gobiet, L. Menut, G. Nikulin, A. Haensler, N. Hempelmann, C. Jones, K. Keuler, S. Kovats, N. Kröner, S. Kotlarski, A. Kriegsmann, E. Martin, E. van Meijgaard, C. Moseley, S. Pfeifer, S. Preuschmann, C. Radermacher, K. Radtke, D. Rechid, M. Rounsevell, P. Samuelsson, S. Somot, J.-F. Soussana, C. Teichmann, R. Valentini, R. Vautard, B. Weber and P. Yiou, 2014. EURO-CORDEX: new high-resolution climate change projections for European impact research. *Regional Environmental Change*, 563–578, doi:10.1007/s10113-013-0499-2.

Johansson, M.M., H. Pellikka, K.K. Kahma and K. Ruosteenoja, 2014. Global sea level rise scenarios adapted to the Finnish coast. *Journal of Marine Systems*, **129**, 35–46, doi:10.1016/j.jmarsys.2012.08.007.

Juhola, S., 2010. Mainstreaming climate change adaptation: the case of multi-level governance in Finland. In: E. C. H. Keskitalo (Ed.), Developing adaptation policy and practice in Europe: multi-level governance of climate change, 149–187, Springer, Dordrecth.

Jylhä, K., H. Tuomenvirta and K. Ruosteenoja, 2004. Climate change projections for Finland during the 21st century. *Boreal Env. Res.*, **9**, 127–152.

Jylhä, K., K. Ruosteenoja, J. Räisänen, A. Venäläinen, H. Tuomenvirta, L. Ruokolainen, S. Saku and T. Seitola, 2009. Arvioita Suomen muuttuvasta ilmastosta sopeutumistutkimuksia varten — ACCLIM-hankkeen raportti 2009 (The changing climate in Finland: estimates for adaptation studies. ACCLIM project report 2009.). Raportteja 2009:4, Ilmatieteen laitos. (In Finnish, extended abstract also in English).

Jylhä, K., M. Laapas, K. Ruosteenoja, L. Arvola, A. Drebs, J. Kersalo, S. Saku, H. Gregow, H.-R. Hannula and P. Pirinen, 2014. Climate variability and trends in the Valkea-Kotinen region, southern Finland: comparisons between the past, current and projected climates. *Boreal Env. Res.*, **19 (suppl. A)**, 4–30.

Jylhä, K., J. Jokisalo, K. Ruosteenoja, K. Pilli-Sihvola, T. Kalamees, T. Seitola, H.M. Mäkelä, R. Hyvönen, M. Laapas and A. Drebs, 2015. Energy demand for the heating and cooling of residental houses in Finland in a changing climate. *Energy and Buildings*, **99**, 104–116, doi:10.1016/j.enbuild.2015.04.001.

Lehtonen, I., K. Ruosteenoja, A. Venäläinen and H. Gregow, 2014. The projected 21st century forest-fire risk in Finland under different greenhouse gas scenarios. *Boreal Environment Research*, **19**, 127–139.

Lind, P. and E. Kjellström, 2008. Temperature and precipitation changes in Sweden, a wide range of model-based projections for the 21st century. Rep. Meteorology and Climatology 113, Swedish Meteorological and Hydrological Inst., Norrköping, Sweden. www.smhi.se/polopoly_fs/1.3297!RMK113_rapport_090421.pdf.

Luomaranta, A., K. Ruosteenoja, K. Jylhä, H. Gregow, J. Haapala and A. Laaksonen, 2014. Multimodel estimates of the changes in the Baltic Sea ice cover during the present century. *Tellus A*, **66**, 22,617, doi:http://dx.doi.org/10.3402/tellusa.v66.22617.

Mäkipää, R., T. Linkosalo, A. Komarov and A. Mäkelä, 2015. Mitigation of climate change with biomass harvesting in Norway spruce stands: are harvesting practices carbon neutral? *Canadian Journal of Forest Research*, **45**, 217–225, doi:10.1139/cjfr-2014-0120.

Meleshko, V.P., V.M. Kattsov, V.A. Govorkova, P.V. Sporyshev, I.M. Shkol'nik and B.E. Shneerov, 2008. Climate of Russia in the 21st century. Part 3. Future climate changes calculated with an ensemble of coupled atmosphere-ocean general circulation CMIP3 models. *Russian Meteorology and Hydrology*, **33**, 541–552, doi:10.3103/S106837390809001X.

Mikkonen, S., M. Laine, H. Mäkelä, H. Gregow, H. Tuomenvirta, M. Lahtinen and A. Laaksonen, 2015. Trends in the average temperature in Finland, 1847–2013. *Stochastic Environmental Research and Risk Assessment*, **29**, 1521–1529, doi:10.1007/s00477-014-0992-2.

Peltonen-Sainio, P., L. Jauhiainen, T. Palosuo, K. Hakala and K. Ruosteenoja, 2015. Rainfed crop production challenges under European high-latitude conditions. *Regional Environmental Change*, doi: 10.1007/s10113-015-0875-1.

Pilli-Sihvola, K., B. van Oort, I. Hanssen-Bauer, M. Ollikainen, M. Rummukainen and H. Tuomenvirta, 2014. Communication and use of climate scenarios for climate change adaptation in Finland, Sweden and Norway. *Local Environment: The Int. Journal of Justice and Sustainability*, doi: 10.1080/13549839.2014.967757.

Pirinen, P., H. Simola, J. Aalto, J.-P. Kaukoranta, P. Karlsson and R. Ruuhela, 2012. Tilastoja Suomen ilmastosta 1981–2010 (Climatological statistics of Finland 1981–2010). Raportteja 2012:1, Ilmatieteen laitos. (In Finnish, abstract in English).

Räisänen, J. and O. Räty, 2013. Projections of daily mean temperature variability in the future: cross-validation tests with ENSEMBLES regional climate simulations. *Clim Dyn*, **41**, 1553–1568, doi:10.1007/s00382-012-1515-9.

Räisänen, J. and J.S. Ylhäisi, 2015. CO2 -induced climate change in northern Europe: CMIP2 versus CMIP3 versus CMIP5. *Climate Dynamics*, **45**, 1877–1897, doi:10.1007/s00382-014-2440-x.

Ruosteenoja, K. and P. Räisänen, 2013. Seasonal changes in solar radiation and relative humidity in Europe in response to global warming. *J. Climate*, **26**, 2467–2481, doi:10.1175/JCLI-D-12-00007.1.

Ruosteenoja, K., K. Jylhä and H. Tuomenvirta, 2005. Climate scenarios for FINADAPT studies of climate change adaptation. No. 345 in Mimeographs, Finnish Environment Institute, Helsinki, Finland. FINADAPT working paper 15.

Ruosteenoja, K., H. Tuomenvirta and K. Jylhä, 2007. GCM-based regional temperature and precipitation change estimates for Europe under four SRES scenarios applying a super-ensemble pattern-scaling method. *Climatic Change*, **81**, 193–208, doi:10.1007/s10584-006-9222-3.

Ruosteenoja, K., J. Räisänen, K. Jylhä, H. Mäkelä, I. Lehtonen, H. Simola, A. Luomaranta and S. Weiher, 2013. Maailmanlaajuisiin CMIP3-malleihin perustuvia arvioita Suomen tulevasta ilmastossa (Climate change estimates for Finland on the basis of global CMIP3 climate models). Raportteja 2013:4, Ilmatieteen laitos. (In Finnish with abstract in English and Swedish).

Ruosteenoja, K., J. Räisänen, A. Venäläinen and M. Kämäräinen, 2015. Projections for the duration and degree days of the thermal growing season in Europe derived from CMIP5 model output. *International Journal of Climatology*, doi:10.1002/joc.4535.

Ruuhela, R., 2011. Miten väistämättömään ilmastonmuutokseen voidaan sopeutua? — Yhteenveto suomalaisesta sopeutumistutkimuksesta eri toimialoilla. Julkaisuja 6-2011, Maa- ja metsätalousministeriö, Helsinki, Finland. (In Finnish).

Sievänen, R., O. Salminen, A. Lehtonen, P. Ojanen, J. Liski, K. Ruosteenoja and M. Tuomi, 2014. Carbon stock changes of forest land in Finland under different levels of wood use and climate change. *Annals of Forest Science*, **71**, 255–265, doi:10.1007/s13595-013-0295-7.

Strandberg, G., L. Bärring, U. Hansson, C. Jansson, C. Jones, E. Kjellström, M. Kolax, M. Kupiainen, G. Nikulin, P. Samuelsson, A. Ullerstig and S. Wang, 2014. CORDEX scenarios for Europe from the Rossby Centre regional climate model RCA4. Rep. Meteorology and Climatology 116, Swedish Meteorological and Hydrological Inst., Norrköping, Sweden. www.smhi.se/polopoly_fs/1.90273!/Menu/general/extGroup/attachmentColHold/mainCol1/file/RMK_116.pdf.

Taylor, K.E., R.J. Stouffer and G.A. Meehl, 2012. An overview of CMIP5 and the experiment design. *Bulletin of the American Meteorological Society*, **93**, 485–498, doi:10.1175/BAMS-D-11-00094.1.

Torssonen, P., H. Strandman, S. Kellomäki, A. Kilpeläinen, K. Jylhä, A. Asikainen and H. Peltola, 2015. Do we need to adapt the choice of main boreal tree species in forest regeneration under the projected climate change? *Forestry*, **88**, 564–572, doi:10.1093/forestry/cpv023.

Turunen, M., S. Rasmus, M. Bavay, K. Ruosteenoja and J. Heiskanen, 2016. Coping with difficult weather and snow conditions: Reindeer herders' views on climate change impacts and coping strategies. *Climate Risk Management*, doi:10.1016/j.crm.2016.01.002.

van Vuuren, D.P., J. Edmonds, M. Kainuma, K. Riahi, A. Thomson, K. Hibbard, G.C. Hurtt, T. Kram, V. Krey, J.-F. Lamarque, T. Masui, M. Meinshausen, N. Nakicenovic, S.J. Smith and S.K. Rose, 2011. The representative concentration pathways: an overview. *Climatic Change*, **109**, 5–31, doi:10.1007/s10584-011-0148-z.

Weigel, A.P., R. Knutti, M.A. Liniger and C. Appenzeller, 2010. Risks of model weighting in multimodel climate projections. *J. Climate*, **23**, 4175–4191.

Yip, S., C.A.T. Ferro, D.B. Stephenson and E. Hawkins, 2011. A simple, coherent framework for partitioning uncertainty in climate predictions. *J. Climate*, **24**, 4634–4643, doi:10.1175/2011JCLI4085.1.

Ylhäisi, J.S., L. Garrè, J. Daron and J. Räisänen, 2015. Quantifying sources of climate uncertainty to inform risk analysis for climate change decision-making. *Local Environment*, **20**, 811–835, doi:10.1080/13549839.2013.874987.

Climate projections for Finland under the RCP forcing scenarios

Kimmo Ruosteenoja, Kirsti Jylhä and Matti Kämäräinen

An attachment file

Table S1. Projected seasonal and annual mean changes in mean surface air temperature (in °C) relative to 1981–2010; spatial averages over Finland (DJF: December to February; MAM: March to May; JJA: June to August; SON: September to November; ANN: annual mean). Projections are given separately for three 30-year future periods and four RCP forcing scenarios. For each projection, three quantiles are given, with the median standing for the best estimate for the change and the 5. and 95. percentage points defining the 90 % probability interval. The quantiles are derived from a normal distribution fitted to the multi-model data (see section 2.3)

Period	Forcing	Quantile	DJF	MAM	JJA	SON	ANN
2020–2049	RCP2.6	5 %	0.5	0.5	0.3	0.4	0.6
2020–2049	RCP2.6	Median	2.0	1.6	1.3	1.5	1.6
2020–2049	RCP2.6	95 %	3.6	2.7	2.2	2.5	2.5
2020–2049	RCP4.5	5 %	0.4	0.6	0.5	0.5	0.7
2020–2049	RCP4.5	Median	2.3	1.9	1.4	1.6	1.8
2020–2049	RCP4.5	95 %	4.3	3.1	2.3	2.7	2.9
2020–2049	RCP6.0	5 %	0.5	0.5	0.5	0.5	0.7
2020–2049	RCP6.0	Median	2.0	1.5	1.2	1.4	1.5
2020–2049	RCP6.0	95 %	3.4	2.5	1.9	2.4	2.4
2020–2049	RCP8.5	5 %	1.0	0.7	0.6	0.9	1.0
2020–2049	RCP8.5	Median	2.7	2.0	1.7	2.0	2.1
2020–2049	RCP8.5	95 %	4.5	3.3	2.8	3.1	3.1
2040–2069	RCP2.6	5 %	0.7	0.8	0.3	0.7	0.8
2040–2069	RCP2.6	Median	2.4	2.0	1.5	1.8	1.9
2040–2069	RCP2.6	95 %	4.2	3.1	2.7	2.9	3.0
2040–2069	RCP4.5	5 %	0.9	0.9	0.8	0.8	1.1
2040–2069	RCP4.5	Median	3.3	2.5	2.0	2.3	2.5
2040–2069	RCP4.5	95 %	5.6	4.2	3.2	3.7	3.9
2040–2069	RCP6.0	5 %	1.0	0.8	0.7	1.0	1.1
2040–2069	RCP6.0	Median	3.0	2.2	1.8	2.1	2.3
2040–2069	RCP6.0	95 %	4.9	3.7	2.9	3.3	3.5
2040–2069	RCP8.5	5 %	2.4	1.6	1.3	1.9	2.1
2040–2069	RCP8.5	Median	4.6	3.2	2.7	3.3	3.5
2040–2069	RCP8.5	95 %	6.8	4.8	4.2	4.7	4.9
2070–2099	RCP2.6	5 %	0.8	0.6	0.3	0.7	0.8
2070–2099	RCP2.6	Median	2.4	1.9	1.5	1.8	1.9
2070–2099	RCP2.6	95 %	4.0	3.1	2.7	2.9	3.0
2070–2099	RCP4.5	5 %	1.7	1.6	1.0	1.4	1.7
2070–2099	RCP4.5	Median	4.3	3.3	2.5	3.1	3.3
2070–2099	RCP4.5	95 %	6.9	5.1	4.0	4.8	4.9
2070–2099	RCP6.0	5 %	2.4	1.9	1.4	1.8	2.1
2070–2099	RCP6.0	Median	4.6	3.5	2.9	3.4	3.6
2070–2099	RCP6.0	95 %	6.8	5.1	4.5	4.9	5.1
2070–2099	RCP8.5	5 %	4.0	3.1	2.3	3.1	3.5
2070–2099	RCP8.5	Median	7.2	5.3	4.6	5.2	5.6
2070–2099	RCP8.5	95 %	10.3	7.5	6.9	7.4	7.7

Table S2. Projected seasonal and annual mean changes in precipitation (in %) for Finland; for further information, see the caption of Table S1.

Period	Forcing	Quantile	DJF	MAM	JJA	SON	ANN
2020–2049	RCP2.6	5 %	-4	-4	-6	-3	0
2020–2049	RCP2.6	Median	6	6	3	6	5
2020–2049	RCP2.6	95 %	16	16	13	14	10
2020–2049	RCP4.5	5 %	-5	-4	-7	-3	-1
2020–2049	RCP4.5	Median	7	7	3	5	5
2020–2049	RCP4.5	95 %	19	17	14	13	12
2020–2049	RCP6.0	5 %	-2	-3	-4	-2	0
2020–2049	RCP6.0	Median	6	5	3	5	5
2020–2049	RCP6.0	95 %	15	12	11	13	9
2020–2049	RCP8.5	5 %	-1	-4	-4	-1	1
2020–2049	RCP8.5	Median	9	7	4	8	7
2020–2049	RCP8.5	95 %	19	18	12	16	13
2040–2069	RCP2.6	5 %	-2	-2	-5	-2	0
2040–2069	RCP2.6	Median	7	7	4	7	6
2040–2069	RCP2.6	95 %	16	15	13	15	11
2040–2069	RCP4.5	5 %	-2	-4	-6	-2	0
2040–2069	RCP4.5	Median	10	8	5	8	7
2040–2069	RCP4.5	95 %	23	20	15	17	14
2040–2069	RCP6.0	5 %	0	-1	-5	1	2
2040–2069	RCP6.0	Median	10	7	3	7	7
2040–2069	RCP6.0	95 %	20	15	12	14	12
2040–2069	RCP8.5	5 %	4	-2	-8	1	3
2040–2069	RCP8.5	Median	17	11	5	12	11
2040–2069	RCP8.5	95 %	30	24	17	23	18
2070–2099	RCP2.6	5 %	-2	-2	-4	-2	1
2070–2099	RCP2.6	Median	7	6	5	7	6
2070–2099	RCP2.6	95 %	17	14	14	15	12
2070–2099	RCP4.5	5 %	2	-3	-5	0	3
2070–2099	RCP4.5	Median	14	11	7	11	11
2070–2099	RCP4.5	95 %	26	25	19	22	18
2070–2099	RCP6.0	5 %	4	2	-6	2	4
2070–2099	RCP6.0	Median	17	12	7	12	12
2070–2099	RCP6.0	95 %	30	21	20	22	19
2070–2099	RCP8.5	5 %	9	3	-12	6	7
2070–2099	RCP8.5	Median	28	18	9	19	18
2070–2099	RCP8.5	95 %	48	33	30	33	28

Table S3. Projected seasonal and annual mean changes in incident solar radiation (in %) for Finland; for further information, see the caption of Table S1.

Period	Forcing	Quantile	DJF	MAM	JJA	SON	ANN
2020–2049	RCP2.6	5 %	-8	-3	-1	-5	-2
2020–2049	RCP2.6	Median	-1	0	2	2	1
2020–2049	RCP2.6	95 %	5	3	6	9	5
2020–2049	RCP4.5	5 %	-10	-4	-1	-5	-2
2020–2049	RCP4.5	Median	-3	0	2	2	1
2020–2049	RCP4.5	95 %	4	4	6	9	4
2020–2049	RCP6.0	5 %	-8	-3	-1	-4	-2
2020–2049	RCP6.0	Median	-2	0	2	2	1
2020–2049	RCP6.0	95 %	4	3	5	8	4
2020–2049	RCP8.5	5 %	-11	-5	-2	-6	-2
2020–2049	RCP8.5	Median	-3	0	2	2	1
2020–2049	RCP8.5	95 %	4	4	6	10	5
2040–2069	RCP2.6	5 %	-9	-3	-2	-5	-2
2040–2069	RCP2.6	Median	-2	0	3	3	2
2040–2069	RCP2.6	95 %	5	3	7	10	5
2040–2069	RCP4.5	5 %	-13	-5	-2	-6	-3
2040–2069	RCP4.5	Median	-4	0	2	2	1
2040–2069	RCP4.5	95 %	4	4	7	11	5
2040–2069	RCP6.0	5 %	-12	-4	-2	-5	-2
2040–2069	RCP6.0	Median	-4	-1	2	2	1
2040–2069	RCP6.0	95 %	3	3	6	10	4
2040–2069	RCP8.5	5 %	-17	-6	-3	-7	-4
2040–2069	RCP8.5	Median	-8	-1	3	2	1
2040–2069	RCP8.5	95 %	2	4	8	12	5
2070–2099	RCP2.6	5 %	-9	-3	-2	-6	-3
2070–2099	RCP2.6	Median	-2	0	2	3	1
2070–2099	RCP2.6	95 %	5	4	7	11	6
2070–2099	RCP4.5	5 %	-16	-6	-4	-9	-4
2070–2099	RCP4.5	Median	-6	-1	2	2	1
2070–2099	RCP4.5	95 %	3	4	9	14	6
2070–2099	RCP6.0	5 %	-16	-6	-4	-8	-5
2070–2099	RCP6.0	Median	-7	-2	2	2	1
2070–2099	RCP6.0	95 %	2	3	8	12	6
2070–2099	RCP8.5	5 %	-26	-11	-6	-11	-7
2070–2099	RCP8.5	Median	-13	-3	3	2	0
2070–2099	RCP8.5	95 %	-1	4	11	16	7

Table S4. Projected seasonal and annual mean changes in the difference between the daily maximum and minimum temperatures (in %) for Finland; for further information, see the caption of Table S1.

Period	Forcing	Quantile	DJF	MAM	JJA	SON	ANN
2020–2049	RCP2.6	5 %	-18	-9	-4	-9	-9
2020–2049	RCP2.6	Median	-8	-3	0	-3	-3
2020–2049	RCP2.6	95 %	1	2	4	4	2
2020–2049	RCP4.5	5 %	-20	-12	-5	-11	-10
2020–2049	RCP4.5	Median	-10	-4	0	-3	-4
2020–2049	RCP4.5	95 %	0	4	5	4	2
2020–2049	RCP6.0	5 %	-16	-9	-4	-9	-8
2020–2049	RCP6.0	Median	-9	-3	0	-3	-4
2020–2049	RCP6.0	95 %	-1	2	3	3	1
2020–2049	RCP8.5	5 %	-21	-11	-5	-12	-10
2020–2049	RCP8.5	Median	-12	-4	-1	-4	-5
2020–2049	RCP8.5	95 %	-2	2	4	3	1
2040–2069	RCP2.6	5 %	-22	-12	-6	-10	-11
2040–2069	RCP2.6	Median	-11	-4	0	-3	-4
2040–2069	RCP2.6	95 %	1	3	6	4	3
2040–2069	RCP4.5	5 %	-28	-17	-7	-14	-14
2040–2069	RCP4.5	Median	-14	-6	0	-4	-6
2040–2069	RCP4.5	95 %	0	6	6	5	3
2040–2069	RCP6.0	5 %	-23	-14	-6	-12	-12
2040–2069	RCP6.0	Median	-13	-5	0	-4	-5
2040–2069	RCP6.0	95 %	-3	4	5	4	2
2040–2069	RCP8.5	5 %	-34	-20	-9	-18	-18
2040–2069	RCP8.5	Median	-20	-8	-1	-6	-8
2040–2069	RCP8.5	95 %	-5	4	7	5	2
2070–2099	RCP2.6	5 %	-22	-12	-7	-10	-11
2070–2099	RCP2.6	Median	-11	-4	0	-3	-4
2070–2099	RCP2.6	95 %	-1	4	6	5	3
2070–2099	RCP4.5	5 %	-37	-22	-11	-20	-20
2070–2099	RCP4.5	Median	-19	-8	-1	-6	-8
2070–2099	RCP4.5	95 %	-1	7	9	8	4
2070–2099	RCP6.0	5 %	-36	-22	-10	-18	-20
2070–2099	RCP6.0	Median	-20	-8	-1	-6	-8
2070–2099	RCP6.0	95 %	-4	6	7	6	3
2070–2099	RCP8.5	5 %	-54	-33	-15	-25	-29
2070–2099	RCP8.5	Median	-30	-12	-2	-9	-13
2070–2099	RCP8.5	95 %	-7	9	11	8	4

Table S5. Projected seasonal and annual mean changes in surface air pressure (in hPa) for Finland; for further information, see the caption of Table S1.

Period	Forcing	Quantile	DJF	MAM	JJA	SON	ANN
2020–2049	RCP2.6	5 %	-2.6	-1.1	-1.1	-1.4	-1.0
2020–2049	RCP2.6	Median	-0.4	-0.0	-0.3	-0.3	-0.2
2020–2049	RCP2.6	95 %	1.9	1.0	0.5	0.9	0.5
2020–2049	RCP4.5	5 %	-2.8	-1.3	-1.1	-1.4	-1.1
2020–2049	RCP4.5	Median	-0.1	-0.0	-0.3	-0.1	-0.1
2020–2049	RCP4.5	95 %	2.6	1.3	0.5	1.2	0.8
2020–2049	RCP6.0	5 %	-2.1	-1.1	-1.0	-1.3	-1.0
2020–2049	RCP6.0	Median	-0.4	-0.1	-0.4	-0.3	-0.3
2020–2049	RCP6.0	95 %	1.3	0.9	0.3	0.7	0.5
2020–2049	RCP8.5	5 %	-2.9	-1.1	-1.4	-1.7	-1.2
2020–2049	RCP8.5	Median	-0.7	0.0	-0.4	-0.5	-0.4
2020–2049	RCP8.5	95 %	1.5	1.2	0.6	0.8	0.4
2040–2069	RCP2.6	5 %	-2.4	-1.1	-1.1	-1.4	-1.0
2040–2069	RCP2.6	Median	-0.2	-0.0	-0.2	-0.2	-0.2
2040–2069	RCP2.6	95 %	2.0	1.1	0.6	0.9	0.7
2040–2069	RCP4.5	5 %	-2.7	-1.4	-1.4	-1.9	-1.2
2040–2069	RCP4.5	Median	-0.3	-0.1	-0.3	-0.4	-0.3
2040–2069	RCP4.5	95 %	2.1	1.3	0.7	1.2	0.7
2040–2069	RCP6.0	5 %	-2.2	-1.2	-1.3	-1.3	-1.0
2040–2069	RCP6.0	Median	-0.4	-0.1	-0.3	-0.4	-0.3
2040–2069	RCP6.0	95 %	1.3	0.9	0.6	0.6	0.4
2040–2069	RCP8.5	5 %	-3.2	-1.5	-1.7	-2.1	-1.4
2040–2069	RCP8.5	Median	-0.8	-0.2	-0.5	-0.5	-0.5
2040–2069	RCP8.5	95 %	1.6	1.1	0.7	1.0	0.5
2070–2099	RCP2.6	5 %	-2.1	-1.1	-1.0	-1.7	-1.0
2070–2099	RCP2.6	Median	-0.2	0.1	-0.3	-0.3	-0.2
2070–2099	RCP2.6	95 %	1.6	1.3	0.5	1.2	0.6
2070–2099	RCP4.5	5 %	-2.6	-1.4	-1.6	-1.8	-1.2
2070–2099	RCP4.5	Median	-0.4	-0.0	-0.5	-0.3	-0.3
2070–2099	RCP4.5	95 %	1.7	1.3	0.6	1.2	0.6
2070–2099	RCP6.0	5 %	-3.0	-1.3	-1.6	-2.0	-1.5
2070–2099	RCP6.0	Median	-0.9	-0.2	-0.6	-0.6	-0.6
2070–2099	RCP6.0	95 %	1.3	1.0	0.3	0.8	0.4
2070–2099	RCP8.5	5 %	-4.1	-2.2	-2.4	-2.9	-2.3
2070–2099	RCP8.5	Median	-1.2	-0.5	-0.8	-1.0	-0.9
2070–2099	RCP8.5	95 %	1.6	1.3	0.8	1.0	0.6

Table S6. Projected seasonal and annual mean changes in surface wind speed (in %) for Finland; for further information, see the caption of Table S1.

Period	Forcing	Quantile	DJF	MAM	JJA	SON	ANN
2020–2049	RCP2.6	5 %	-6	-8	-3	-5	-5
2020–2049	RCP2.6	Median	0	-1	0	0	0
2020–2049	RCP2.6	95 %	6	6	3	5	4
2020–2049	RCP4.5	5 %	-7	-8	-3	-5	-5
2020–2049	RCP4.5	Median	0	-1	0	-1	0
2020–2049	RCP4.5	95 %	7	6	3	3	4
2020–2049	RCP6.0	5 %	-5	-6	-3	-4	-4
2020–2049	RCP6.0	Median	0	0	0	0	0
2020–2049	RCP6.0	95 %	6	5	4	4	4
2020–2049	RCP8.5	5 %	-7	-10	-5	-6	-7
2020–2049	RCP8.5	Median	1	-1	0	1	0
2020–2049	RCP8.5	95 %	8	9	6	8	7
2040–2069	RCP2.6	5 %	-9	-10	-5	-7	-7
2040–2069	RCP2.6	Median	-1	-1	0	0	0
2040–2069	RCP2.6	95 %	8	8	5	7	6
2040–2069	RCP4.5	5 %	-9	-11	-5	-7	-7
2040–2069	RCP4.5	Median	0	-1	-1	-1	-1
2040–2069	RCP4.5	95 %	8	8	3	6	6
2040–2069	RCP6.0	5 %	-9	-10	-4	-6	-7
2040–2069	RCP6.0	Median	0	-1	0	0	0
2040–2069	RCP6.0	95 %	9	9	5	6	7
2040–2069	RCP8.5	5 %	-10	-14	-7	-9	-10
2040–2069	RCP8.5	Median	1	0	0	1	0
2040–2069	RCP8.5	95 %	12	13	8	10	10
2070–2099	RCP2.6	5 %	-11	-12	-6	-8	-9
2070–2099	RCP2.6	Median	-1	-1	0	0	-1
2070–2099	RCP2.6	95 %	8	9	6	8	7
2070–2099	RCP4.5	5 %	-11	-14	-7	-9	-9
2070–2099	RCP4.5	Median	-1	-2	-1	-1	-1
2070–2099	RCP4.5	95 %	9	9	5	7	7
2070–2099	RCP6.0	5 %	-13	-15	-6	-9	-10
2070–2099	RCP6.0	Median	-1	-1	0	0	-1
2070–2099	RCP6.0	95 %	12	12	5	9	9
2070–2099	RCP8.5	5 %	-17	-18	-9	-12	-14
2070–2099	RCP8.5	Median	0	-1	-1	1	0
2070–2099	RCP8.5	95 %	18	17	8	14	14

Table S7. Projected seasonal changes (means of parallel runs) in six climate variables from 1981–2010 to 2070–2099 under the RCP4.5 scenario as simulated by the individual models; spatial averages over Finland. DJF: December to February; MAM: March to May; JJA: June to August; SON: September to November.

Model	Temperature (°C)				Precipitation (%)				Pressure (hPa)				Radiation (%)				Temp. range (°C)				Wind speed (%)			
	DJF	MAM	JJA	SON	DJF	MAM	JJA	SON	DJF	MAM	JJA	SON	DJF	MAM	JJA	SON	DJF	MAM	JJA	SON	DJF	MAM	JJA	SON
MIROC5	4.1	4.0	3.0	3.4	5	8	6	15	1.4	0.4	-0.3	-0.3	1	2	4	6	-0.9	-0.1	0.2	-0.0	-1	2	1	-1
MIROC-ESM	4.8	5.3	3.9	4.0	18	29	15	16	-1.2	-0.7	-0.2	-1.3	-12	-5	5	4	-1.0	-0.5	-0.0	-0.3	-22	-27	1	-22
MIROC-ESM-CHEM	6.1	5.9	4.1	4.2	21	21	19	23	-1.4	1.3	-0.8	-1.4	-13	-5	5	5	-1.2	-0.5	-0.0	-0.2	-11	-26	1	-17
MRI-CGCM3	4.9	2.7	1.6	2.6	9	16	21	11	-0.0	0.8	-1.3	-0.4	-8	-4	-3	-6	-1.7	-1.5	-0.8	-0.5	-4	-5	0	0
BCC-CSM1-1	5.7	3.3	1.7	2.7	16	2	13	11	-0.8	1.0	-1.1	-0.2	-14	-1	-2	5	-1.6	-0.8	-0.1	-0.2	5	1	0	2
INMCM4	3.3	2.6	1.0	1.7	8	10	17	6	-0.9	0.4	-1.5	-0.9	-5	-4	-2	-2	-0.9	-1.2	-1.3	-0.8	-2	-1	3	3
NorESM1-M	3.9	3.1	2.9	3.0	16	8	-5	18	-1.4	-0.8	0.3	-1.8	-2	3	7	7	-1.0	0.2	0.7	-0.1	–	–	–	–
NorESM1-ME	3.2	3.2	2.6	2.7	13	8	2	16	-0.2	-0.4	-0.2	-0.5	-3	5	3	4	–	–	–	–	–	–	–	–
HadGEM2-ES	4.5	3.8	3.4	3.8	16	10	5	5	0.6	1.4	-0.3	0.3	-4	1	4	6	-1.1	-0.2	-0.4	-0.2	-4	-7	-5	-4
HadGEM2-CC	5.3	5.0	3.0	4.4	15	18	2	8	-0.9	-0.8	-0.7	0.1	-5	-1	4	6	-1.4	-0.5	-0.4	-0.2	-10	-8	-6	-3
MPI-ESM-LR	3.1	2.6	1.2	2.0	14	6	3	10	0.2	0.3	-0.8	-0.0	-12	-6	-3	-9	-0.9	-0.8	-0.2	-0.4	-5	-7	-7	-4
MPI-ESM-MR	3.4	2.4	1.6	1.8	16	5	5	2	-0.7	-0.4	-0.2	-0.0	-10	-2	-1	-6	-1.1	-0.6	-0.1	-0.4	-5	-7	-5	-6
CNRM-CM5	3.9	3.7	2.7	2.8	8	22	3	-2	0.3	-1.0	0.0	1.2	7	0	5	7	-0.5	-0.4	-0.1	-0.1	2	0	0	-4
IPSL-CM5A-LR	6.3	3.6	3.6	4.1	25	0	15	9	0.3	0.1	-1.1	-0.8	-13	3	4	8	–	–	–	–	3	-3	-3	-2
IPSL-CM5A-MR	5.2	3.1	3.0	3.8	20	-8	1	9	-1.1	0.2	-0.6	0.6	-17	7	3	9	–	–	–	–	2	-4	-1	0
CMCC-CM	8.4	5.1	1.9	5.5	36	15	14	18	-0.6	0.1	-2.3	-1.2	-12	-5	-7	-17	-2.7	-2.3	-0.6	-1.3	0	-2	1	1
CMCC-CMS	6.6	4.6	2.9	5.0	13	8	11	23	-0.4	0.5	-0.5	-2.0	-8	-4	5	-20	-2.3	-1.8	-0.0	-1.1	-2	0	1	3
GFDL-CM3	4.5	4.6	4.6	4.0	22	27	13	20	-2.1	-0.9	-0.6	-1.5	-10	-5	12	4	-1.1	-1.0	-0.0	-0.2	13	16	5	9
GFDL-ESM2M	2.7	2.0	1.4	2.4	21	11	4	12	-2.9	0.7	-0.8	-0.3	-5	-3	0	-4	-0.5	-0.8	-0.3	-0.2	8	3	2	4
GISS-E2-R	4.1	1.9	1.7	2.2	12	1	11	7	-0.2	0.6	-0.3	0.0	-5	-2	0	1	-0.4	-0.2	-0.2	-0.3	0	-1	-1	0
GISS-E2-H	5.1	3.2	2.4	2.9	14	12	8	8	-0.6	-0.3	-0.2	-0.3	-12	-3	1	0	-0.6	-0.4	-0.2	-0.3	-3	-2	-3	-2
CCSM4	1.8	1.9	2.3	2.0	3	5	-4	8	0.9	-0.0	0.3	0.3	-5	-1	3	1	-0.6	-0.0	0.4	-0.1	–	–	–	–
CESM1-CAM5	1.4	3.1	3.3	2.4	9	17	2	11	0.4	-0.8	0.3	0.2	11	4	9	19	-0.4	0.5	0.8	0.6	-4	0	1	-2
CESM1-BGC	2.3	2.6	2.4	1.8	5	10	-5	3	0.4	-1.7	0.5	0.4	-5	-2	4	6	-0.7	-0.1	0.5	0.1	–	–	–	–
CanESM2	5.3	3.6	3.5	3.8	14	15	6	16	-0.2	-0.1	-0.6	0.0	-8	-2	4	2	-1.4	-1.0	0.1	-0.3	-1	1	-5	-4
ACCESS1-0	2.8	1.9	2.3	2.6	10	19	0	13	-0.1	-0.6	-0.9	0.3	0	0	2	6	-0.5	0.1	0.1	0.0	0	-1	3	3
ACCESS1-3	3.8	2.8	2.8	2.4	19	19	3	16	-1.8	-0.3	-0.1	-0.8	-5	0	6	9	-0.3	0.3	0.4	0.3	5	2	3	4
EC-EARTH	2.8	2.8	2.0	2.4	3	15	8	4	1.2	-0.4	0.1	0.4	-1	0	1	1	-0.7	-0.3	-0.3	-0.3	-3	-1	-1	-1

Table S8. As in Table S7, but for the RCP8.5 scenario.

Model	Temperature (°C)				Precipitation (%)				Pressure (hPa)				Radiation (%)				Temp. range (°C)				Wind speed (%)			
	DJF	MAM	JJA	SON	DJF	MAM	JJA	SON	DJF	MAM	JJA	SON	DJF	MAM	JJA	SON	DJF	MAM	JJA	SON	DJF	MAM	JJA	SON
MIROC5	6.9	6.7	5.5	5.6	13	14	8	19	1.2	0.6	-0.6	-0.8	-6	1	4	7	-1.5	-0.1	0.3	0.0	-4	-2	-5	-5
MIROC-ESM	8.2	8.4	6.8	6.4	46	32	17	27	-3.4	-0.8	-0.7	-2.3	-27	-7	8	3	-1.4	-0.6	0.2	-0.3	-23	-28	-4	-24
MIROC-ESM-CHEM	9.5	9.2	6.9	6.7	41	28	20	24	-1.6	1.3	-1.0	-1.1	-26	-8	7	5	-1.7	-0.7	0.1	-0.3	-22	-37	-1	-26
MRI-CGCM3	7.6	4.5	3.5	5.2	21	24	37	20	-1.2	-1.0	-2.2	-0.7	-15	-7	-4	-10	-2.5	-2.4	-1.2	-1.0	-7	-9	-1	1
BCC-CSM1-1	8.7	5.1	3.5	4.3	27	16	6	14	-0.3	-0.0	-0.7	-1.3	-17	-8	0	-2	-2.4	-1.4	0.0	-0.5	5	2	-1	1
INMCM4	5.3	4.1	2.3	3.2	12	20	27	5	-1.3	0.2	-2.3	-0.6	-8	-6	-3	-2	-1.7	-1.8	-1.6	-0.9	-4	0	1	-1
NorESM1-M	6.2	4.6	5.5	4.3	23	13	-13	17	-0.9	-0.3	0.8	-1.6	-5	3	11	10	-1.7	0.1	1.1	-0.0	–	–	–	–
NorESM1-ME	6.5	4.6	5.2	4.3	35	17	-4	20	-4.3	-2.1	0.2	-1.5	-6	2	7	9	–	–	–	–	–	–	–	–
HadGEM2-ES	7.5	6.0	6.1	6.5	28	15	-5	13	0.8	1.2	-0.4	0.3	-9	0	6	8	-1.8	-0.2	-0.2	-0.2	-4	-8	-6	-2
HadGEM2-CC	9.1	7.2	6.0	7.3	31	21	-2	25	-0.1	0.2	-1.1	-0.7	-10	-1	5	4	-2.1	-0.5	-0.3	-0.3	-9	-11	-6	0
MPI-ESM-LR	5.3	4.3	2.8	4.2	27	9	4	18	-0.0	0.4	-1.5	-1.1	-20	-7	-6	-11	-1.7	-1.1	-0.3	-0.5	-4	-7	-5	-2
MPI-ESM-MR	6.2	3.8	2.6	4.1	37	14	0	5	-2.0	-1.2	-0.4	-0.3	-17	-7	-6	-4	-1.7	-1.0	-0.2	-0.4	-1	-4	-4	-2
CNRM-CM5	5.9	4.7	3.4	3.9	17	23	18	10	-0.1	0.9	-0.1	0.6	1	-2	-1	2	-0.8	-0.6	-0.9	-0.4	1	-1	0	0
IPSL-CM5A-LR	10.3	6.2	6.6	7.0	52	1	28	23	-1.4	-1.2	-1.8	-1.2	-28	6	5	10	–	–	–	–	8	-1	-6	-2
IPSL-CM5A-MR	7.8	4.3	5.3	5.6	37	-5	23	28	-3.5	-1.1	-2.4	-2.1	-26	5	2	9	–	–	–	–	6	-1	-5	0
CMCC-CM	11.1	7.6	3.3	7.9	49	40	16	35	-0.6	-2.9	-2.6	-1.7	-20	-13	-8	-22	-3.9	-3.4	-0.7	-1.6	0	4	1	3
CMCC-CMS	10.9	7.0	4.6	7.4	43	9	14	29	-2.0	-0.4	-1.0	-2.4	-25	-9	1	-18	-3.4	-2.6	-0.2	-1.3	0	0	-1	5
GFDL-CM3	7.0	6.5	6.9	6.5	38	36	18	28	-4.0	-1.4	-0.8	-3.7	-17	-8	14	11	-1.3	-1.4	-0.2	-0.1	30	29	13	24
GFDL-ESM2M	5.8	4.2	3.3	4.4	28	19	8	28	-3.8	-0.1	-0.3	-1.5	-9	-6	1	-7	-1.2	-1.1	-0.4	-0.4	21	18	12	19
GISS-E2-R	7.8	4.2	3.5	4.4	26	23	18	13	-1.0	-1.1	-1.0	0.2	-12	-8	-1	2	-1.1	-0.6	-0.2	-0.4	0	2	-2	0
GISS-E2-H	8.1	5.5	4.4	5.1	24	16	20	17	-0.6	-0.9	-1.0	-0.5	-18	-6	-1	0	-0.9	-0.5	-0.2	-0.4	-3	-2	-4	-2
CCSM4	4.5	3.8	4.3	3.7	13	12	-4	16	0.1	-0.7	0.0	-0.2	-12	-2	4	2	-1.4	-0.1	0.4	-0.2	–	–	–	–
CESM1-CAM5	4.2	4.7	5.3	4.8	26	21	2	19	-2.0	-0.9	0.2	-0.4	7	3	8	19	-0.9	0.3	0.5	0.5	0	4	4	1
CESM1-BGC	4.5	4.6	4.0	3.7	13	17	1	13	-0.3	-1.6	0.4	1.5	-17	-3	2	4	-1.4	0.1	0.3	0.0	–	–	–	–
CanESM2	7.6	5.7	6.4	6.2	21	27	-2	25	-0.8	-0.9	-1.4	-0.6	-15	-5	8	7	-2.1	-1.6	0.4	-0.3	2	5	-5	-5
ACCESS1-0	6.6	5.4	5.4	5.3	32	19	-13	22	-2.0	-1.0	-1.0	-1.4	-8	0	6	6	-1.1	-0.1	0.6	0.1	3	1	2	5
ACCESS1-3	6.1	4.7	5.0	4.4	39	22	1	25	-1.9	0.6	0.8	-2.3	-13	0	8	11	-0.8	0.3	0.5	0.3	4	1	2	3
EC-EARTH	4.5	4.7	3.4	4.2	10	21	11	10	1.6	0.2	0.0	0.9	-5	-3	-1	1	-1.3	-0.7	-0.3	-0.4	-8	-1	-1	-1

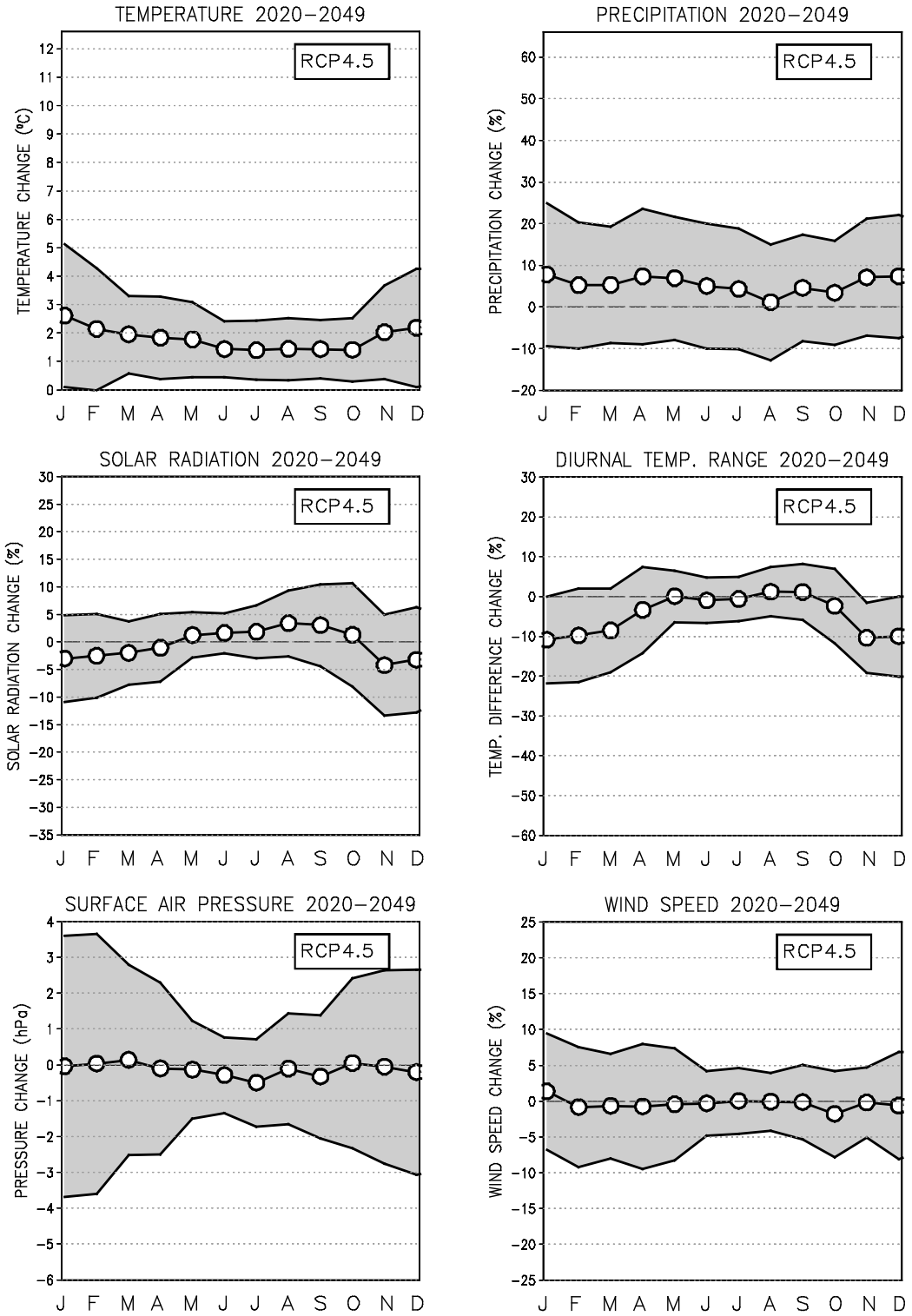

Fig. S1. Projected changes in mean surface air temperature (in °C, top left), precipitation (in %, top right) incident solar radiation (in %, middle left), diurnal temperature range (in %, middle right), surface air pressure (in hPa, bottom left) and wind speed (in %, bottom right) in Finland under the RCP4.5 scenario for the period 2020–2049, relative to 1981–2010. The multi-model mean projections for the various months (J = January, F = February, ...), based on simulations performed with 24–28 climate models, have been denoted by open circles. Grey shading shows the 90 % uncertainty intervals for the change.

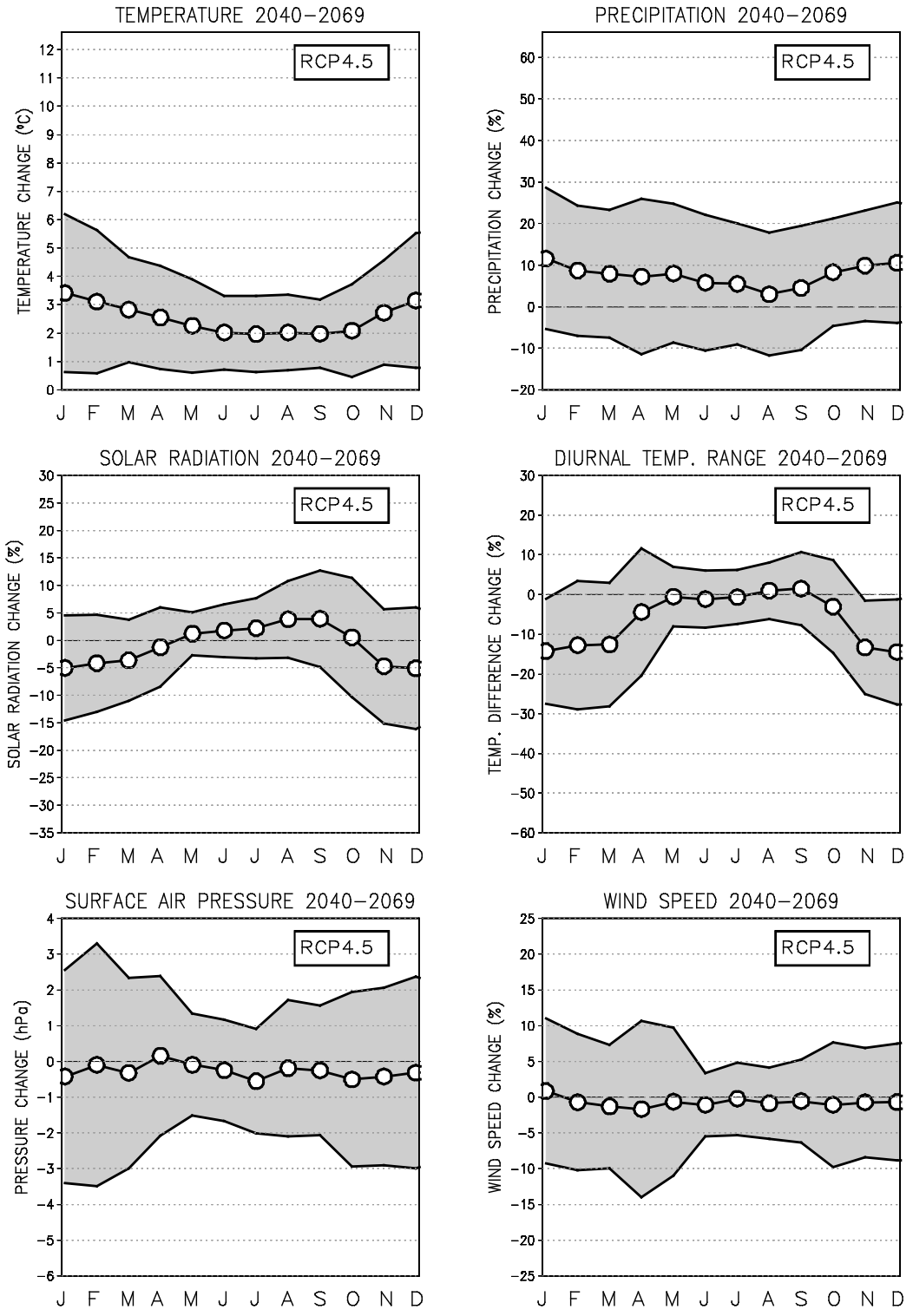

Fig. S2. As in Fig. S1, but for the period 2040–2069.

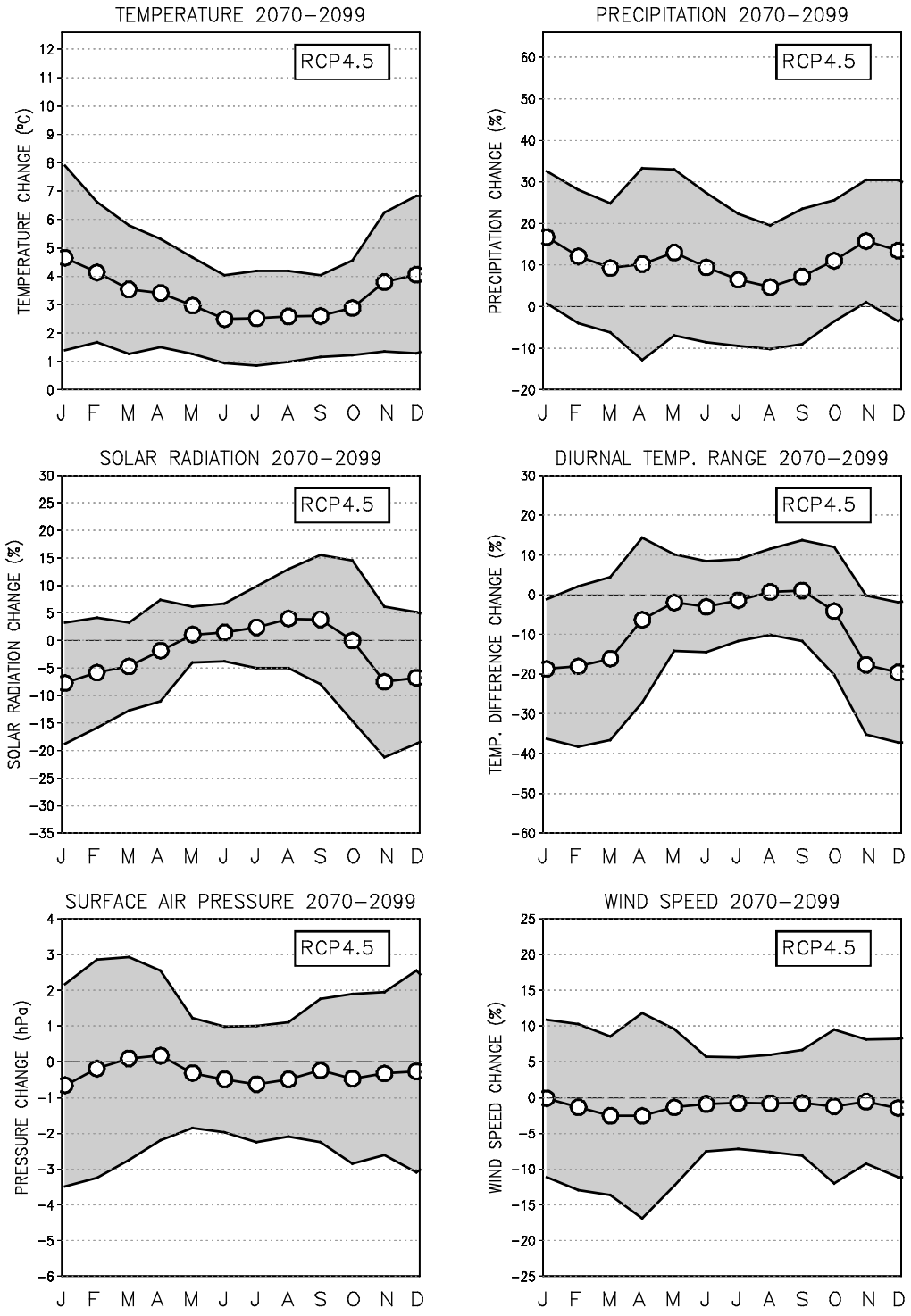

Fig. S3. As in Figs. S1–S2, but for the period 2070–2099 (note the same vertical axis scale in all these figures).

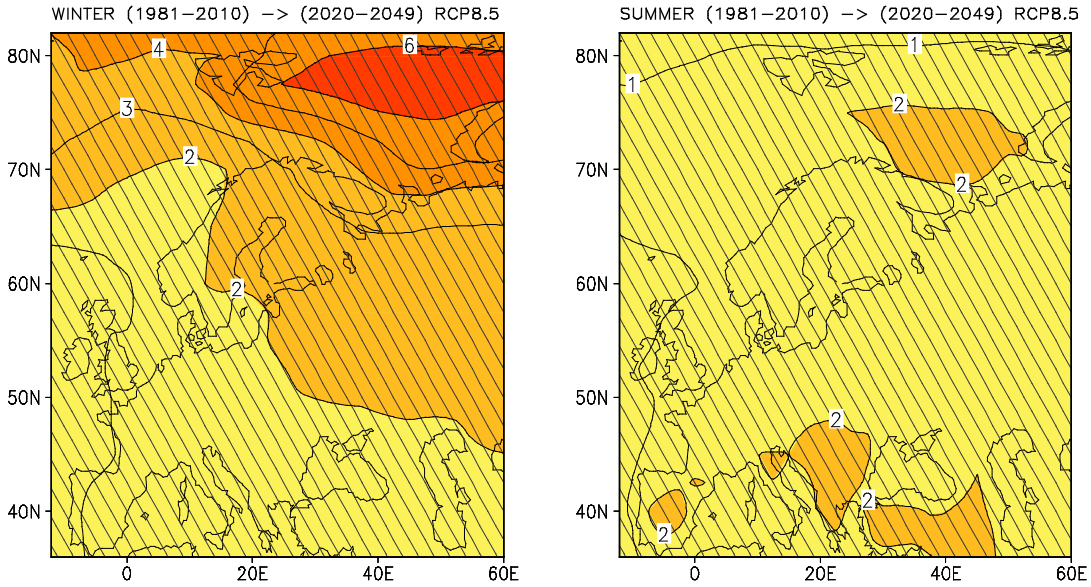

Fig. S4. Projected changes in December-February (left) and June-August (right) mean surface air temperature (in °C) in Europe under the RCP8.5 scenario for the period 2020–2049, relative to 1981–2010; an average of the simulations performed with 28 GCMs. Areas where more than 75 % of the models agree on the sign of change are hatched (for temperature, this condition is fulfilled over the entire domain).

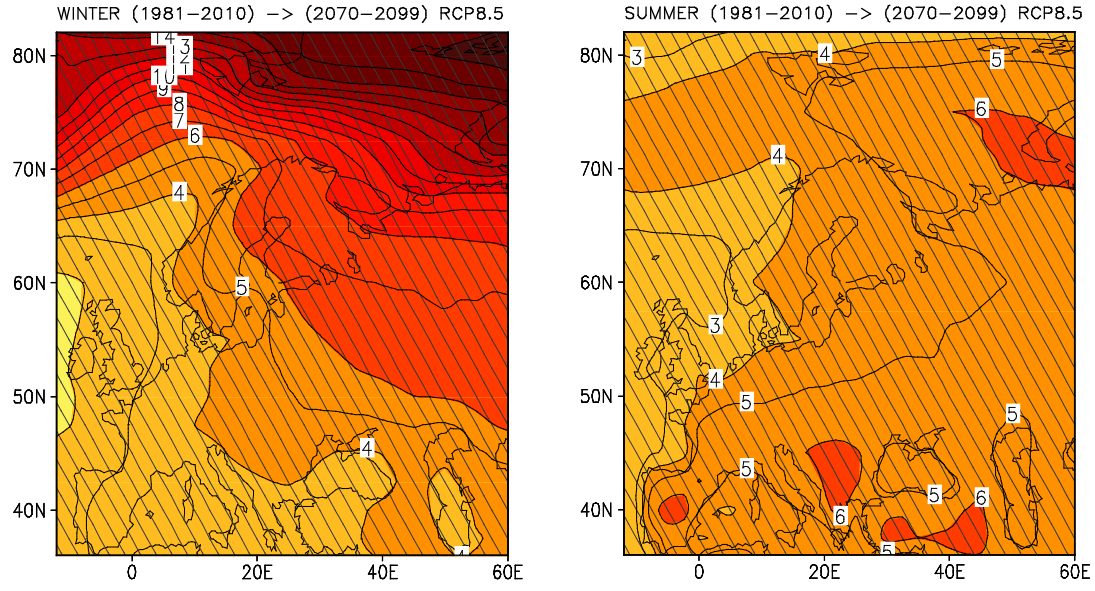

Fig. S5. Projected changes in mean temperature (in °C) in Europe under the RCP8.5 scenario for the period 2070–2099; for further details, see the caption of Fig. S4.

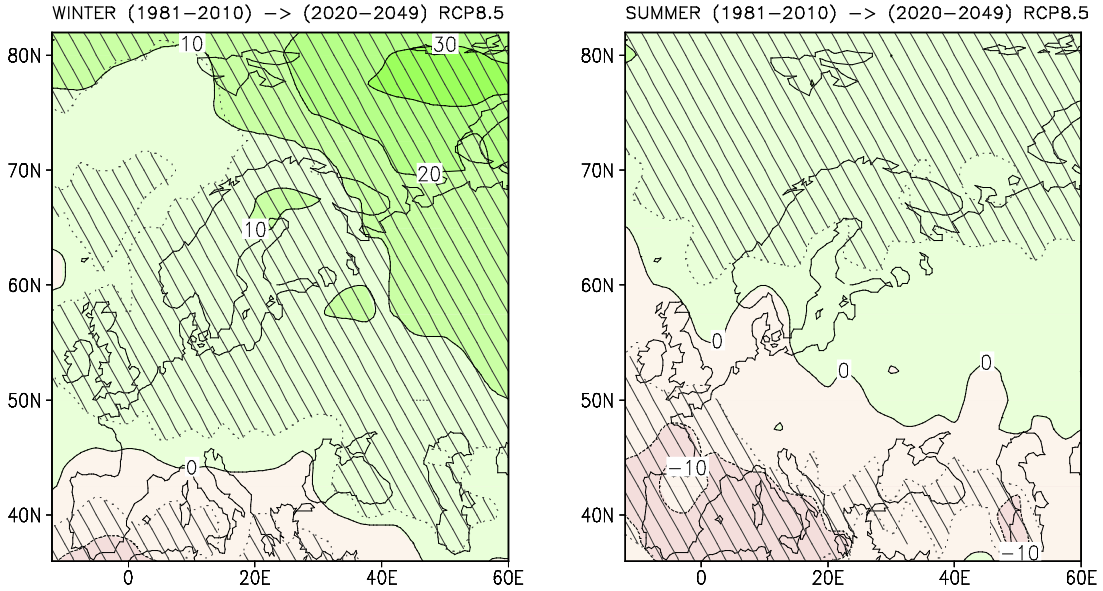

Fig. S6. Projected changes in December–February (left) and June-August (right) precipitation totals (in %) under the RCP8.5 scenario for the period 2020–2049; for further information, see the caption of Fig. S4.

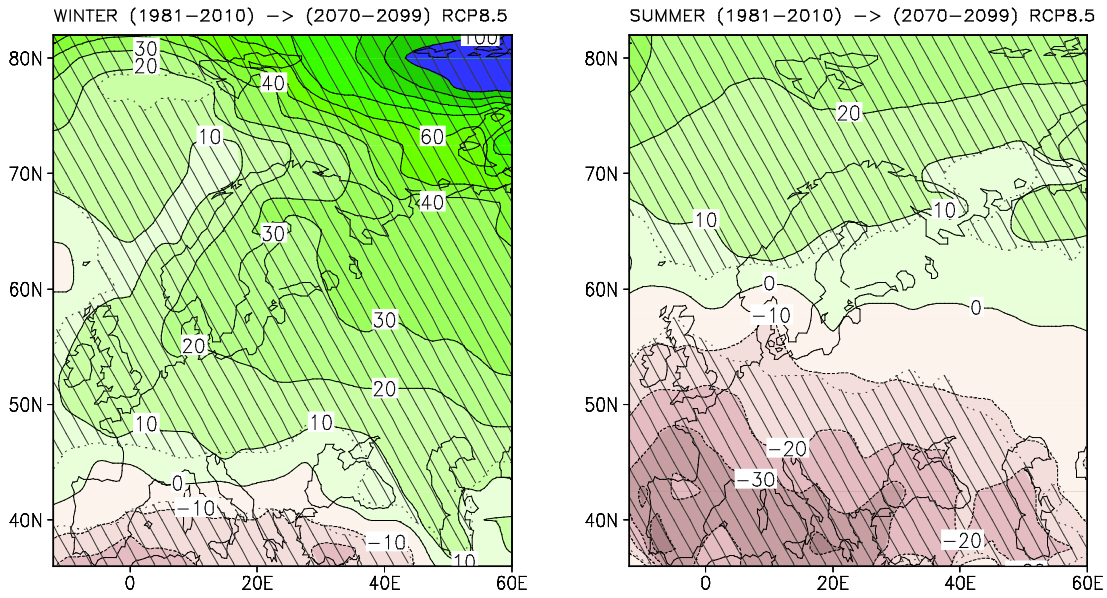

Fig. S7. As Fig. S6 but for the period 2070–2099.

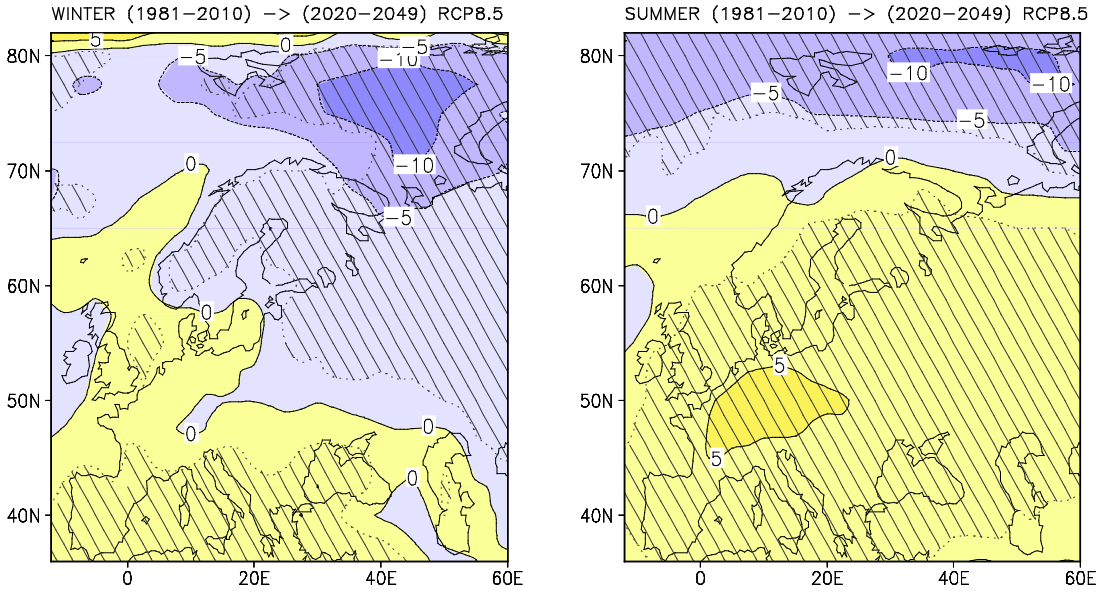

Fig. S8. Projected changes in December-February (left) and June-August (right) incident solar radiation (in %) under the RCP8.5 scenario for the period 2020–2049 (see the caption of Fig. S4).

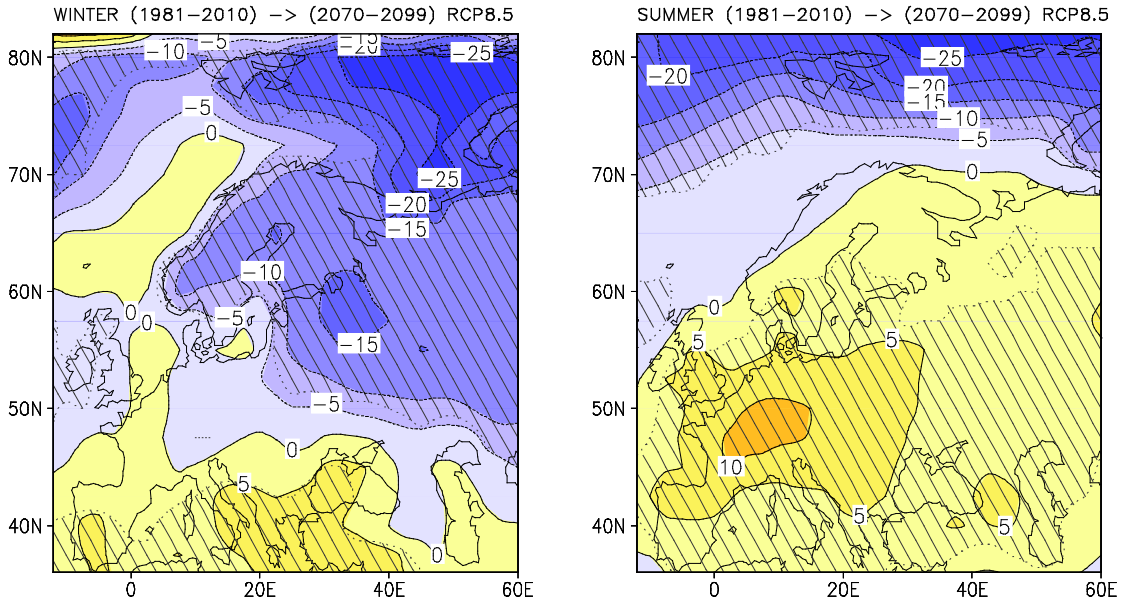

Fig. S9. As Fig. S8 but for the period 2070–2099.

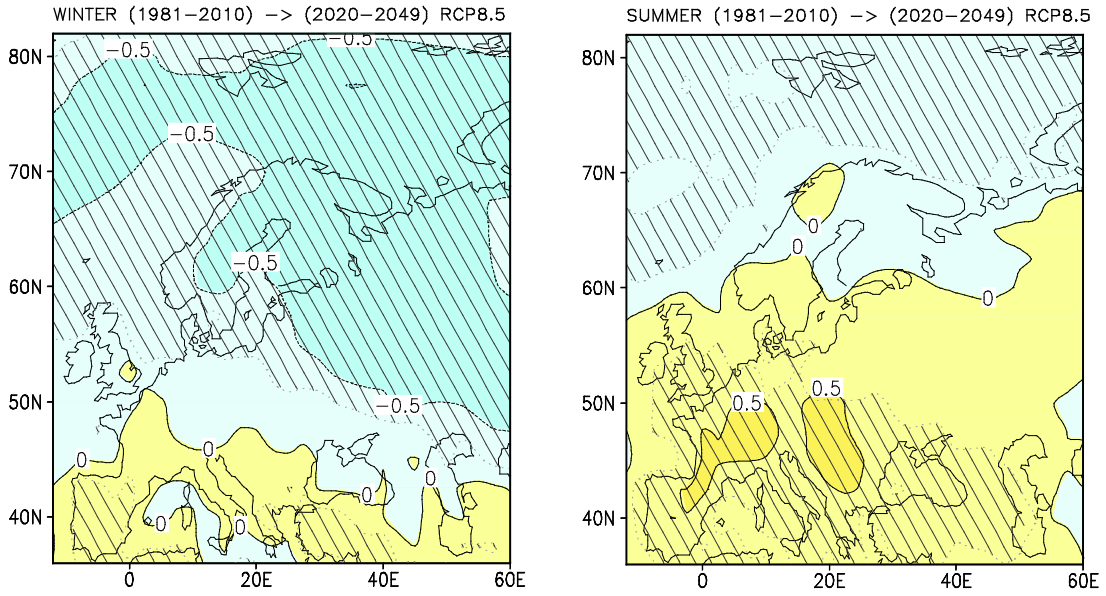

Fig. S10. Projected changes in the difference between the daily maximum and minimum temperatures (in °C) for December–February (left) and June-August (right) under the RCP8.5 scenario for the period 2020–2049; an average of simulations performed with 25 GCMs (see the caption of Fig. S4).

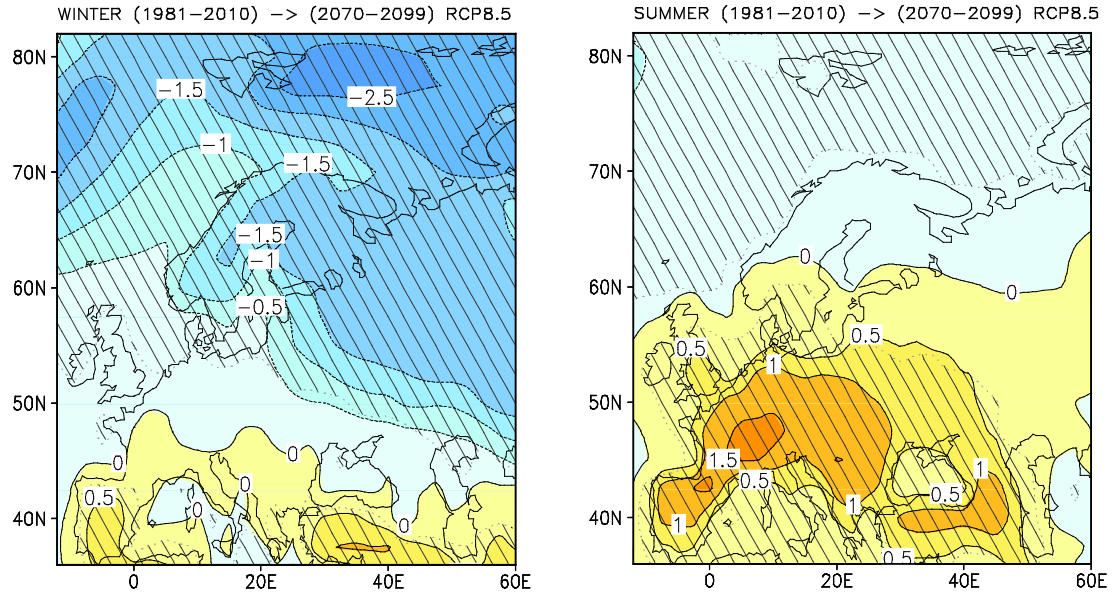

Fig. S11. As Fig. S10 but for the period 2070–2099.

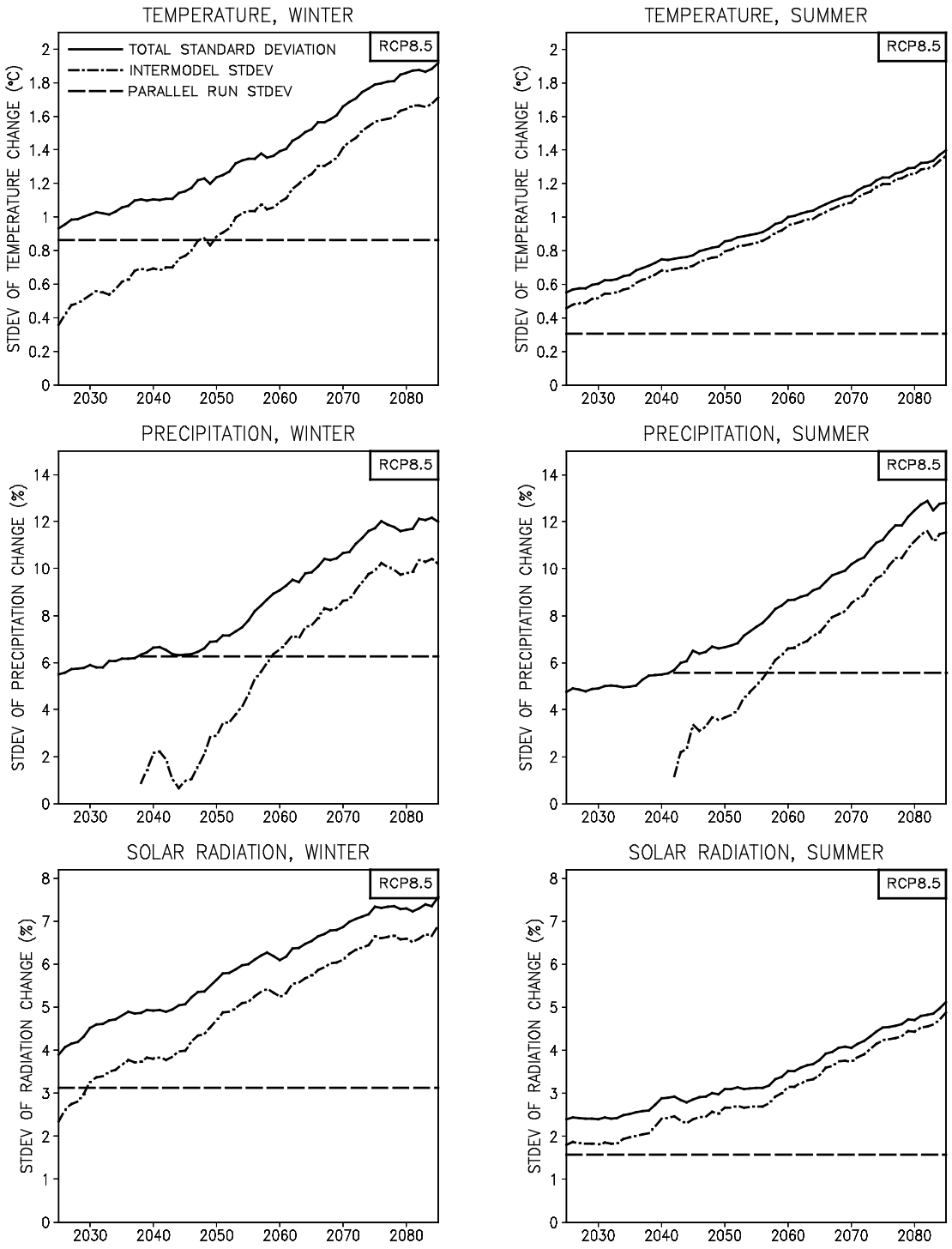

Fig. S12. Temporal evolution of the standard deviation describing uncertainty in the 30-year running mean change in mean temperature (in °C, top), precipitation (in %, middle) and incident solar radiation (in %, bottom) in Finland under the RCP8.5 scenario. Left panels show the uncertainties for December-February, right panels for June-August. The total uncertainty (solid curves) has been decomposed into contributions arising from the true inter-model differences (dash-dotted curves) and differences between the parallel runs (dashed horizontal line); the latter serves as an estimate for internal variability.

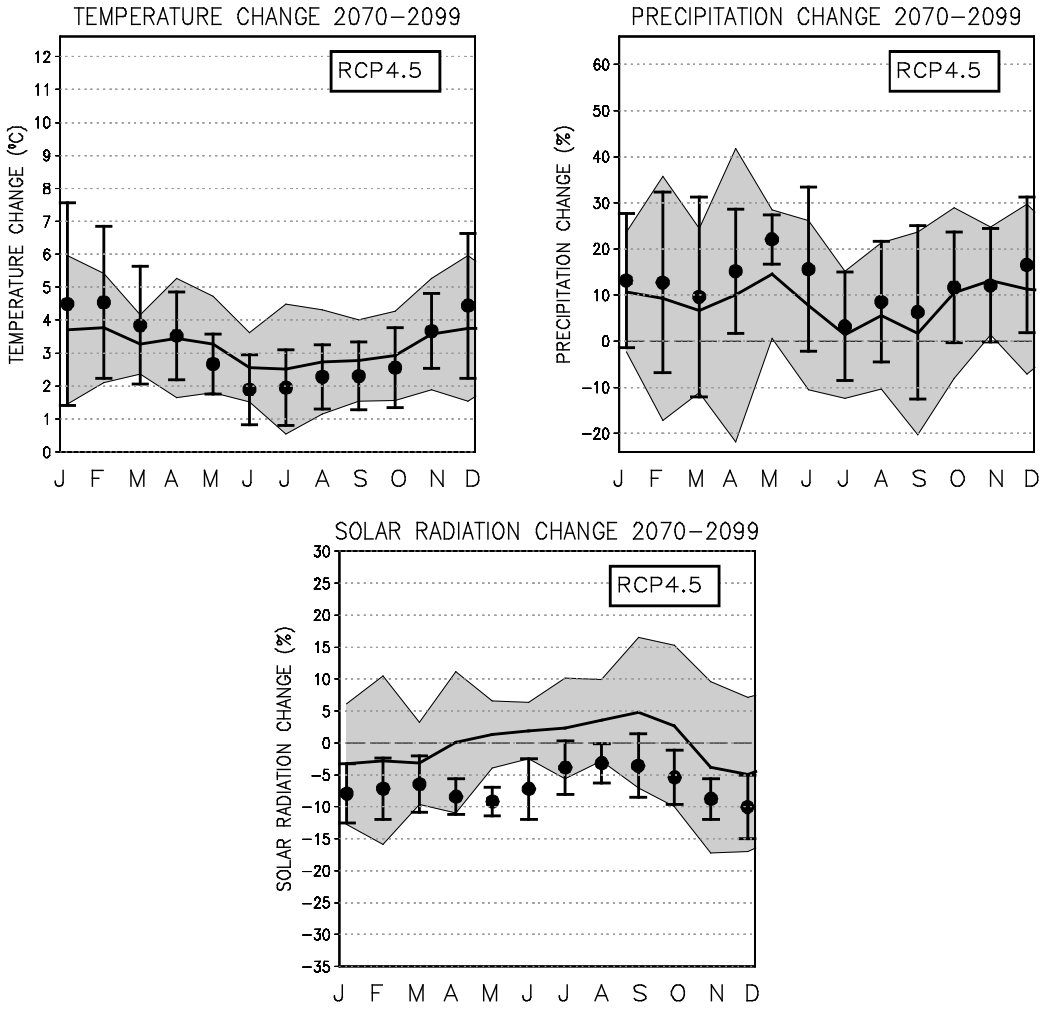

Fig. S13. Monthly-mean changes in temperature (in °C, top left), precipitation (in %, top right) and incident solar radiation (in %, bottom) in Finland for the period 2070–2099 (relative to 1981–2010) under RCP4.5 as inferred from nine driving GCMs and from the corresponding simulations downscaled by the RCA4 regional model. The mean of the projections produced by the driving GCMs has been denoted by a thick curve, grey shading showing the 90 % uncertainty interval for the GCM-derived change. The average of the RCM responses have been denoted by bullets and the corresponding uncertainty intervals by vertical bars.

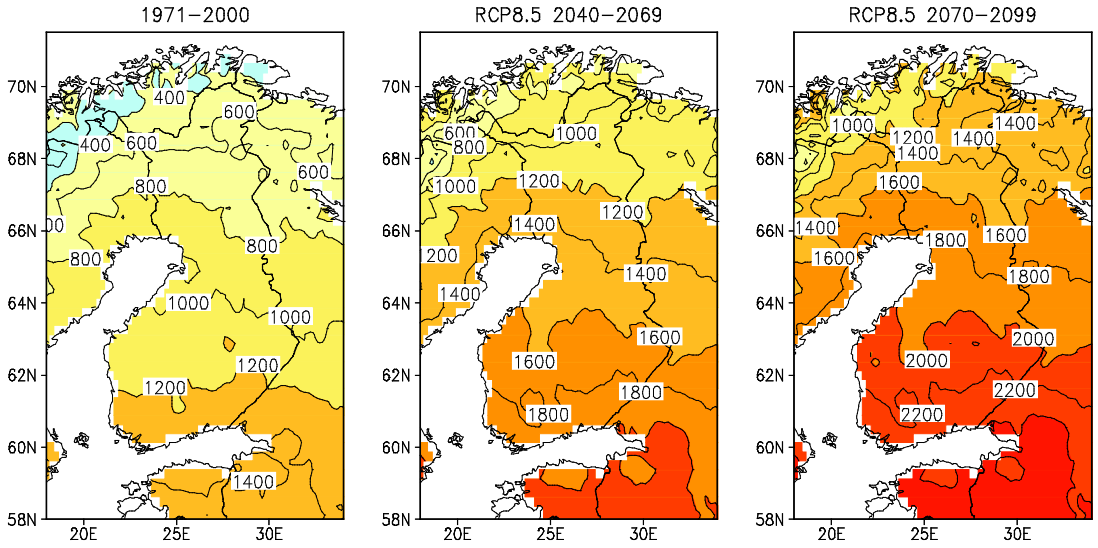

Fig. S14. Temperature sums of the growing season: a time mean for the baseline period (years 1971–2000; left) and future projections (middle: 2040–2069; right: 2070–2099) under the RCP8.5 scenario. Contour interval is 200 degree days. This is a fine-scale representation extracted from Fig. S13 of Ruosteenoja et al. (2015).